Mineralogical Magazine, May 2018, Vol. 82(S1), pp. S199–S222

Textural and mineral-chemistry constraints on columbite-group minerals in the Penouta deposit: evidence from magmatic and fluid-related processes

P. Alfonso[1,*], S. A. Hamid[1], M. Garcia-Valles[2], T. Llorens[3,4], F. J. López Moro[3,4], O. Tomasa[1], D. Calvo[1], E. Guasch[1], H. Anticoi[1], J. Oliva[1], D. Parcerisa[1] and F. García Polonio[3,4]

[1] Departamento d'Enginyeria Minera, Industrial i TIC, Universitat Politècnica de Catalunya, Av de les Bases de Manresa 61-73, 08242 Manresa, Spain
[2] Departamento de Cristalografia, Mineralogia i Dipòsits Minerals, Universitat de Barcelona, Carrer Martí i Franquès, s/n, 08028 Barcelona, Spain
[3] Strategic Minerals Spain, S.L., P° Recoletos, 37, 28004 Madrid, Spain
[4] Dept. of Geology, University of Salamanca, Plaza de los Caídos s/n, 37008 Salamanca, Spain

[*Received 16 January 2017; Accepted 23 December 2017; Associate Editor: Eimear Deady*]

ABSTRACT

The Penouta Sn-Ta deposit, in the northwest of Spain, is a greisenized granitic cupola where Ta minerals occur mainly as disseminations in a leucogranite body intruded in Precambrian–Lower Cambrian gneisses and mica-schists. This leucogranite is a medium- to fine-grained inequigranular rock consisting mainly of quartz, albite, K-feldspar and muscovite. Accessory minerals are mainly of spessartine, zircon, cassiterite, Nb-Ta oxides, monazite, xenotime, native bismuth and pyrite. The alteration processes were mainly albitization, muscovitization and kaolinitization.

This leucogranite is peraluminous and P-poor, with 0.03–0.07 wt.% P_2O_5, 900–1500 ppm Rb, 30–65 ppm Cs, 120–533 ppm Li, 80–140 ppm Ta, 51–81 ppm Nb and up to 569 ppm of Sn.

Mineralogical characterization of Nb-Ta oxide minerals was determined by X-ray diffraction, scanning electron microscopy, electron microprobe analysis and mineral liberation analysis. Mn-rich members of the columbite-group minerals (CGM) are the most common Ta-bearing phases, but microlite, wodginite, tapiolite and Ta-rich cassiterite occur also. CGM crystals are commonly zoned concentrically, with a Nb-rich core surrounded by a Ta-rich rim, with a sharp boundary between them. Convoluted zoning occurs also. Dissolution textures resulting from the corrosion of columbite and tantalite rims, in particular, are common. The Mn/(Mn + Fe) ratio varies between 0.33 and 0.97 and the Ta/(Ta + Nb) ratio between 0.07 and 0.93. Wodginite and microlite formed as late replacements of CGM and occur associated with tantalite and cassiterite. Subhedral to anhedral cassiterite crystals, usually up to 200 μm across, occur in two generations: the earlier one is Nb,Ta-poor whereas in the later generation, the Ta content can reach >9 wt.% of Ta_2O_5 and 1.7 wt.% of Nb. The presence of a fluid phase in the apical zone of the granite, probably related to the separation of a fluid/vapour of the melt, could explain the sponge-like textures, the Ta enrichment associated with these textures, the occurrence of Ta-enriched mineral phases (microlite and wodginite) and their common interstitial character.

*E-mail: maria.pura.alfonso@upc.edu
https://doi.org/10.1180/minmag.2017.081.107

Keywords: tantalum, columbite–tantalite, microlite, wodginite.

This paper is part of a special issue entitled 'Critical-metal mineralogy and ore genesis'. The Applied Mineralogy Group of the Mineralogical Society and the IMA Commission on Ore Mineralogy have contributed to the costs of Open Access publication for this paper.

Introduction

New technologies, leading to the miniaturization of electronic devices, have resulted in the increased use of tantalum. Use of tantalum-based capacitors, in particular, is on the increase in automotive electronics, mobile phones, personal computers and wireless devices (Mackay and Simandl, 2014). On the other hand, there is an increasing interest in Ta in terms of the ethical aspects involved in its extraction. A significant amount of the Ta produced comes from non-sustainable operations. Around 62% of the world's tantalum supply comes from Africa, particularly from Burundi, Democratic Republic of Congo (DRC) and Rwanda (Roskill, 2016), where its exploitation can cause conflicts (such as war) and involves child labour (Smith *et al*., 2012). Brazil and China also contribute to the global tantalum supply, with ~19% of the supply coming from the Pitinga and Mibra mines in Brazil, and ~12% of supply coming from the Yichun granite in China. The tantalum market has important ethical aspects that should be taken into account when considering sustainable exploitation (Bleischwitz *et al*., 2012) and new sources should be developed to diversify geographic sources of supply for strategic reasons (Mackay and Simandl, 2014).

Traditionally, the majority of tantalum was exploited from pegmatites. However, rare-metal granites also contain significant amounts of this metal (Černý *et al*., 2005; Linnen *et al*., 2014) and have been studied extensively (Cuney *et al*., 1992; Helba *et al*., 1997; Belkasmi and Cuney, 1998; Rub *et al*., 1998; Belkasmi *et al*., 2000; Huang *et al*., 2002; Stepanov *et al*., 2014; Melcher *et al*., 2015). The scarcity of this metal makes it essential that further research, on granites, be done.

In addition, several aspects related to the genesis of Ta ore deposits remain unsolved. The transport and fractionation of Ta in the magmatic-hydrothermal transition, and the possible influence of subsolidus processes in Ta precipitation, in pegmatites and granites, have generated considerable controversy. Many authors consider that Ta has an affinity for melt, as supported by experimental results (Linnen and Keppler, 1997; Linnen, 1998; London, 2008) and field evidence in pegmatites (Dewaele *et al*., 2015) and granites (Huang *et al*., 2015; López Moro *et al*., 2017). Other cases provide evidence that late exsolved hydrothermal fluids during the late stages of magmatic crystallization are responsible for the Ta-richest mineralization (Belkasmi and Cuney, 1998; Dostal *et al*., 2015; Neiva *et al*., 2015; Zhu *et al*., 2015). This hypothesis was maintained by evidence from the textures of Nb-Ta oxide minerals from granites and pegmatites (Zhu *et al*., 2015). Therefore, the study of Nb-Ta mineralization in granites is of great interest from both an economical and scientific point of view.

The rare-metal granite at Penouta is a Sn, Ta-rich leucogranite that belongs to the Sn-W European Variscan belt. In the Iberian Massif this belt contains abundant W, Sn and Ta deposits (e.g. Gonzalo Corral and Gracía Plaza, 1985; Charoy and Noronha, 1996; Llorens and Moro, 2010, 2012; Canosa *et al*., 2012; Chicharro *et al*., 2015; Llorens González *et al*., 2017; López Moro *et al*., 2017).

The Penouta deposit was exploited from Roman times until 1985 (IGME, 1976). The re-opening of this deposit is now being investigated. The measured and indicated resources are reported to be 95.5 Mt with an average grade of 77 ppm Ta and 443 ppm Sn (Llorens González *et al*., 2017). The aim of the present study was to present a mineralogical and geochemical study of Sn and Nb-Ta minerals in this granite in order to determine the influence of magmatic and hydrothermal processes on the formation of this mineralization.

Geological setting

The Penouta deposit is located in the Central Iberian Zone of the Iberian Variscan Massif, near the contact with the Asturoccidental–Leonese Zone (Fig. 1), according to the classification of Julivert *et al*. (1972). In the Central Iberian Zone the Variscan orogeny generated most of the extant structures, the internal deformation and the metamorphism. During the first Variscan deformation phase (D_1), a low-grade slaty cleavage (S_1) and recumbent folds were developed in the northern domain of the CIZ. The second Variscan deformation event yielded thrusting toward the external zones, crustal anatexis and a pervasive subhorizontal tectonic foliation (S_2) linked to extension in the internal domains. The Variscan D_3 phase led to upright folds, open to tight folds and occasionally a crenulation cleavage (S_3) associated with subvertical shear zones with a dextral wrench component (Iglesias and Choukroune, 1980).

The Penouta deposit is located in the hinge of a D_1 Variscan antiform (Fig. 1) that is obliterated by the D_3 Ollo de Sapo anticlinorium. This megastructure follows a NW–SE direction (Fig. 1) and forms a continuous outcrop that extends ~300 km, from the island of Coelheira (Lugo) to the point where it disappears under the Tertiary materials of

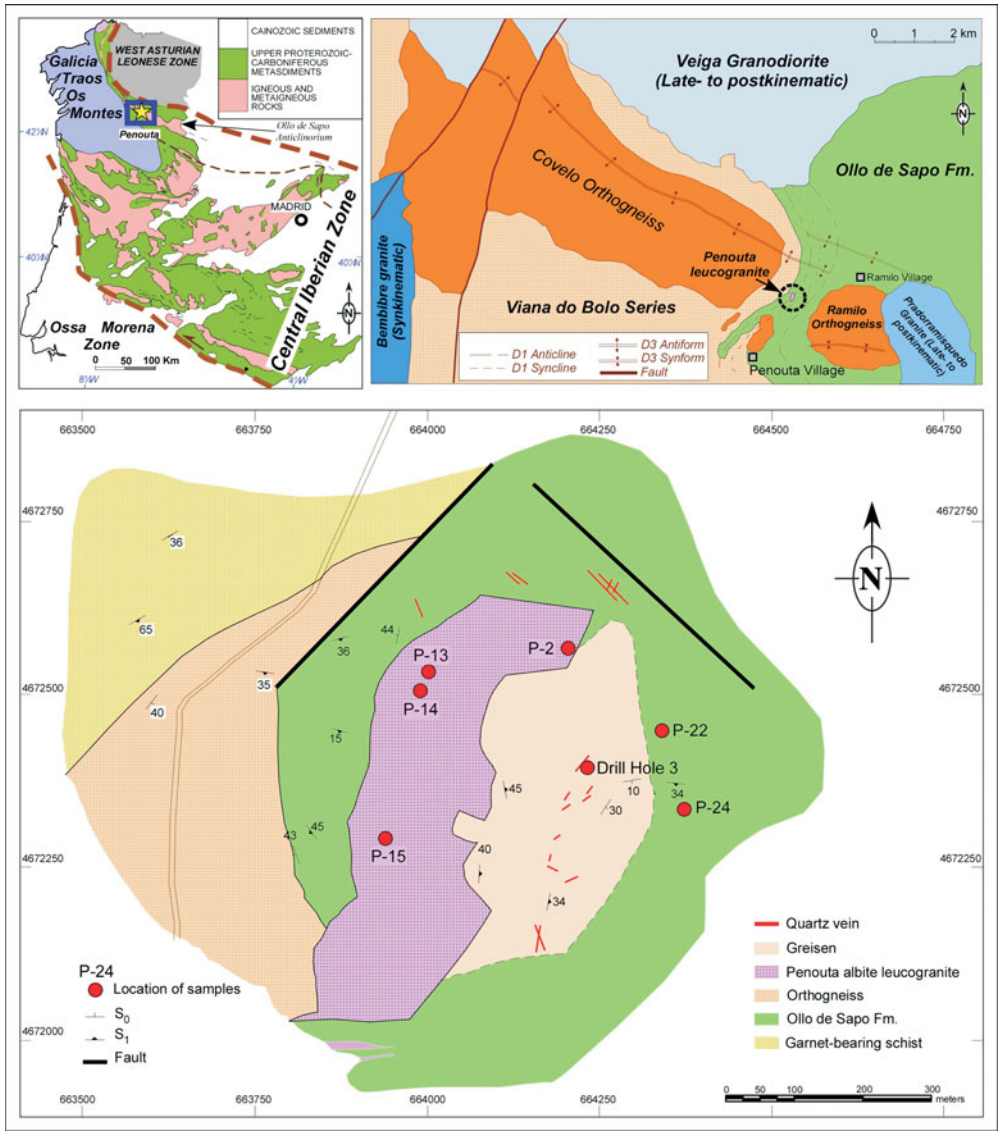

FIG. 1. Detailed geological map of the Penouta deposit showing the locations of the samples. Upper left: location of Penouta in the Iberian Variscan Massif; upper right: geological sketch of the Ollo de Sapo Anticlinorium in its western region (modified from López Moro *et al.*, 2017).

the Duero Basin (Arribas and Mangas, 1991; Arias *et al.*, 2002) (Fig. 1).

The metamorphic rocks of the area consist of a lower part which crops out in the core of a gneiss dome around the Viana do Bolo village, the so-called Viana do Bolo Series (Ferragne, 1972); this is overlain by the Ollo de Sapo Formation. The Viana do Bolo Series constitutes the oldest material in the area and is a metamorphic complex consisting of quartzites, followed by mica-schists with garnet and Ca-silicate rocks which crop out NE of Penouta, and orthogneisses deformed during the Variscan orogeny, which crop out in the Covelo and Ramilo localities, near Penouta (Díez Montes, 2006) (Fig. 1). The lower part of the series is considered to be Lower Cambrian (Arias *et al.*,

2002) but the age of the upper part is not well known and a range of ages from Middle Cambrian to the lowermost Ordovician has been reported (Díez *et al*., 2010). These materials are overlain by the Ollo de Sapo Formation, which is a volcanogenic sequence consisting of fine- to coarse-grained massive gneisses with ocellar texture.

With regard to igneous rocks in the area, synkinematic granites are scarce and crop out close to Viana do Bolo village (Bembibre granite), whereas late to post-kinematic granodiorites (Veiga Granodiorite) and granites (Pradorramisquedo granite) are more important volumetrically (Fig. 1).

The Penouta deposit is a greisenized cupola with four units: albite leucogranite, aplite-pegmatite dykes, greisen and quartz veins hosted in the metamorphic country rock (Llorens González *et al*., 2017). The Penouta stock is a leucogranitic body that intruded the Viana do Bolo Series and Ollo de Sapo Formation. Study of the outcrops has revealed that the granite intruded following planar anisotropies developed in the country rock corresponding to the regional D_2 Variscan fabric. There are no ages available for the Penouta granite and only a relative dating can be inferred from structural and contact relationships. The lack of foliation and significant internal deformation in this body are features typical of the late- to post-Variscan, similar to the Veiga and Pradorramisquedo plutons (Fig. 1), which have been inferred to be related to a strike-slip shear zone (Vegas *et al*., 2001), this stage being similar in age (~308 Ma, Gutiérrez-Alonso *et al*., 2015) to other Sn-bearing granites dated recently in the CIZ (e.g. Logrosán Sn-(W) ore deposit, 308 ± 1 Ma, Chicharro *et al*., 2015).

The Penouta albite granite is similar in composition to other albite granites in the Iberian Massif, most of them located in the innermost part of the Iberian Variscan Belt, namely, in the Central Iberian Zone. Most of these albite leucogranites were affected by an intense albitization, kaolinitization and greisenization (Mangas and Arribas, 1991; Clauer *et al*., 2015), probably related to fluid saturation in the apical zone of the leucogranite (López Moro *et al*., 2017).

Analytical methods

Granite samples were obtained from the ancient open pit of the Penouta mine (Fig. 1), corresponding to the apical zone. Whole-rock samples were analysed by Activation Laboratories (ACTLABS), Ontario, Canada. Major elements were analysed by X-ray fluorescence (XRF). Minor elements were measured using inductively coupled plasma-mass spectrometry (ICP-MS) from acid digestion of fused glass beads. Fusion was obtained using lithium or sodium borate. More details of sample preparation and analysis can be found in ACTLABS (2017).

Petrographic and mineralogical characterizations were carried out by powder X-ray diffraction (XRD), optical microscopy and scanning electron microscopy (SEM). The XRD spectra were measured from powdered samples in a Bragg-Brentano PANAnalytical X'Pert Diffractometer (graphite monochromator, automatic gap, *K*α-radiation of Cu at λ = 1.54061 Å, powered at 45 kV–40 mA, scanning range 4–100° with a 0.017°2θ step scan and a 50 s measuring time. Identification and Rietveld semi-quantitative evaluation of phases were done using the PANanalytical *X'Pert HighScore* software.

Scanning electron microscopy with energy-dispersive spectral analysis (SEM–EDS) was used in back-scattered electron (BSE) mode. Electron microprobe analysis was used to establish the chemistry of the minerals. Analyses were carried out using a JEOL JXA-8230 electron microprobe located at the Centres Cientifics i Tecnològics de la Universitat de Barcelona. Analyses were conducted at an accelerating voltage of 20 kV, an electron beam current of 20 nA, and a beam diameter of 2 μm. Each element was counted for 5 s, except Ti, Sc and Pb, which were counted for 10 s and F for 15 s. Standards used were: Nb (Nb*L*α), Ta (Ta*L*α), Fe_2O_3 (Fe*K*α), rhodonite (Mn*K*α), rutile (Ti*K*α), ThO_2 (Th*M*α), UO_2 (U*M*β), Sn (Sn*L*α), W (W*L*α), Sc (Sc*K*α), albite (Na*K*α), apatite (F*K*α), wollastonite (Ca*K*α), galena (Pb*M*α), ZrO_2 (Zr*L*α) and YAG (Y*L*α). The detection limits are 0.17 wt.% U, 0.1 wt.% Y, Th and W, 0.06 wt.% Ta, Sn and Nb and <0.03 wt.% for other elements. The structural formulae were calculated on the basis of 24 oxygens and 12 cations per formula unit (apfu) for CGM. The number of cations was fixed by a method of charge balance by conversion of part of Fe^{2+} to Fe^{3+} as proposed by Ercit *et al*. (1992*a*). The structural formula of tapiolite and cassiterite were calculated on the basis of 6 and 4 oxygens, respectively. The structural formula of microlite was calculated on the basis of a fully occupied B site (Nb + Ta + W + Ti = 2 apfu) and OH^- was calculated by charge-balancing to the anion total of 7 (Černý *et al*., 2004). The wodginite formula was calculated according to the general formula ABC_2O_8 ($Z = 4$); $A = Mn^{2+}$, Fe^{2+}, Li, □, $B = Sn^{4+}$,

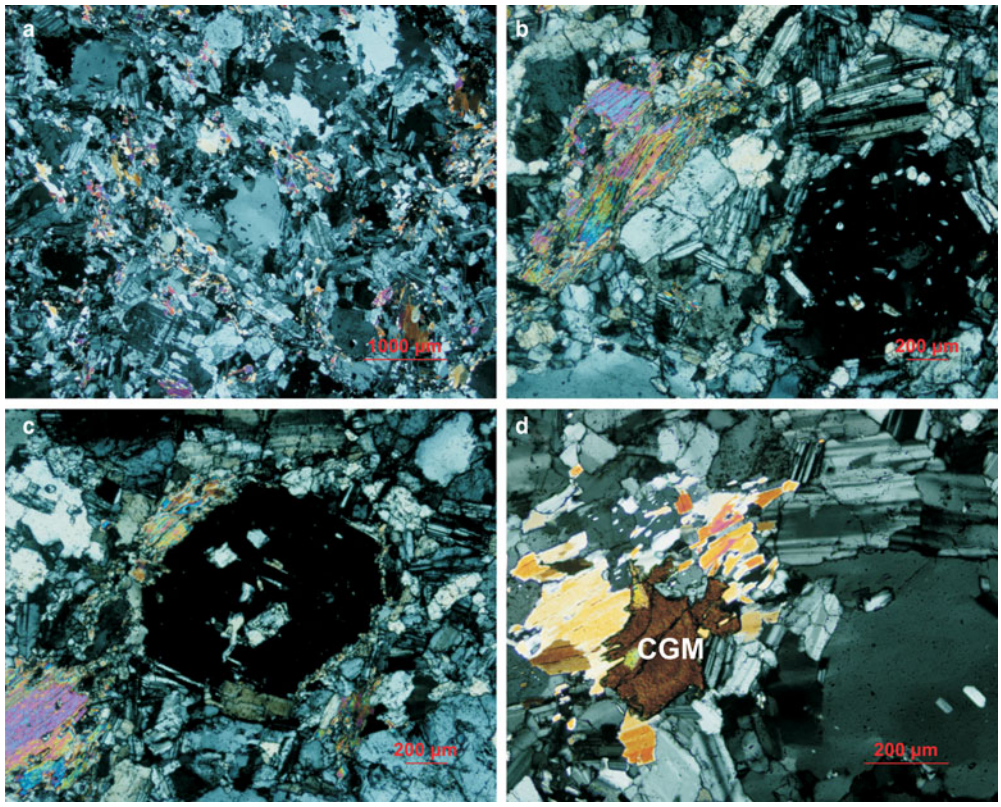

FIG. 2. Transmitted light photomicrographs of the Penouta granite: (*a*) general view of the porphyritic texture; (*b*,*c*) details of the snowball texture of quartz; (*d*) columbite-group crystal (CGM) associated with muscovite.

Ti, Fe^{3+}, Ta; *C* = Ta, Nb (Ercit *et al*. 1992*a*,*b*,*c*). When the *C* site had >2 apfu, the excess was corrected by extraction of Ta to the *B* site. The Fe^{3+} was calculated for the *B* site (Ti + Sn^{4+} + Zr + Hf + Fe^{3+}) fully occupied, with 1 apfu.

Mineral liberation analysis (MLA) was performed on a polished section prepared with a concentrated sample at the University of Tasmania using an FEI MLA 650 ESEM to obtain textural and compositional information from a large number of particles.

Results

Petrography and geochemistry of the leucogranite

The Penouta leucogranite is a phaneritic inequigranular rock, with fine to medium grain size. It consists of quartz, albite, white mica and microcline, as essential constituents. The XRD analyses indicate that quartz varies from 15 to 67 wt.%, albite from 2 to 40 wt.%, muscovite from 8 to 35 wt.%, microcline from 4 to 18 wt.%, and there is sporadic kaolinite.

Accessory minerals are spessartine, almandine, tourmaline, cassiterite, Nb-Ta oxides, beryl, apatite, monazite, xenotime, zircon, rutile, pyrite and native bismuth, fluorite, uraninite, Fe, Mn oxides, stannite, molybdenite, chalcopyrite and arsenopyrite.

Quartz occurs at least in two generations, the first of which is euhedral to subhedral crystals in a snowball texture, 0.8–2 mm in size, similar to other rare-metal granites (Charoy and Noronha, 1996; Helba *et al*., 1997; Abdalla *et al*., 1998; Huang *et al*., 2002; Zhu *et al*., 2015). Quartz phenocrysts are rich in mineral inclusions consisting mainly of albite but also of other minerals, such as muscovite, arranged concentrically along growth planes (Fig. 2). The second generation of quartz consists of anhedral grains of <3 mm in size. Zircon also occurs as euhedral crystals that are typically zoned.

The feldspars are mainly albite. Most of the K-feldspar found is microcline with euhedral

crystals, up to 2 mm in size, which often exhibit tartan twinning. Preliminary microprobe analyses of microcline yield up to 1.1 wt.% of Rb_2O and up to 0.17 wt.% of Cs_2O.

Two generations of white micas are distinguished. The first generation consists of Rb- and Cs-poor small crystals and the second generation is consists of much larger crystals, of ~0.5–1 mm in size, and shows textures of replacement. EDS analyses reveal greater contents of incompatible elements in this this second generation, as Rb_2O and Cs_2O.

A widespread albitization and kaolinitization is common throughout the leucogranite outcrops. Kaolinite represents ~5–10 wt.% of all minerals, but locally can reach up to 50 wt.%.

The major- and trace-element compositions of the Penouta leucogranite and the associated greisen from the open pit are given in Table 1. The leucogranite is peraluminous, with an A/(CNK) (Al_2O_3/CaO + Na_2O + K_2O) index of 1.8, and P-poor, with 0.03–0.07 wt.% P_2O_5. However, in the greisen this can reach as much as 0.32 wt.% P_2O_5. The SiO_2 content varies between 69 and 75 wt.%, whereas in the kaolinitic alteration and in the greisen it is less, up to 67.39 wt.%. The Na_2O content of leucogranite varies between 4 and 6 wt.%.

The Li content in the leucogranite is 80–226 ppm, whereas in the greisen it is greater, between 420 and 614 ppm. The Rb content is 900–1500 ppm in the leucogranite and 696–2730 in the greisen and Cs is 30–65 ppm and 29.7–180 ppm, respectively. The Ta and Nb contents are less in the greisen relative to the granite; in the leucogranite the Ta contents are 81–140 ppm, Nb = 51–81 ppm and Sn up to 569 ppm and in the greisen, Ta is 6.3–85.5 ppm, Nb = 9–65.3 ppm and Sn = 4.5–1900 ppm.

The Mg/Li ratio is a good indicator of the degree of fractionation of granites and pegmatites, being in the range 1.7–50 for fertile granites (Selway *et al*., 2005). This ratio in the Penouta leucogranite ranges from 0.8 to 1.9, indicative of a fertile granite (Černý, 1989; Selway *et al*., 2005).

According to Černý (1989) and Selway *et al*. (2005) the K/Rb in fertile granites is 42–270, and the K/Cs 1600–15,400. These criteria are exceeded by the results from the Penouta leucogranite for which K/Rb is 26.6–31.9 and K/Cs is 402–788, both indicative of even higher fertility. In addition the greisen has a Nb/Ta ratio >1.

Mineralogy and chemistry of Nb-Ta-Sn oxides

Columbite-group minerals are the most abundant Nb-Ta rich phases in the Penouta leucogranite although tapiolite, microlite and wodginite occur also. Cassiterite can also contain significant amounts of Nb and Ta. Although Nb-Ta oxide minerals can occur in the greisen and pegmatites from the Penouta deposit (Llorens González *et al*., 2017), they occur mainly in the leoucogranite, and only these are presented here.

Columbite-group minerals

Columbite-group minerals occur as platy crystals usually <200 μm in size, with an average size of 80 μm. Crystals usually constitute isolated grains but are occasionally associated with quartz, muscovite, plagioclase, cassiterite, zircon and other Nb-Ta rich minerals such as wodginite and microlite.

These minerals usually exhibit a zoned texture with Nb-rich cores and Ta-rich rims (Figs 3, 4). Occasionally this zonation is progressive, but in other cases there is a sharp boundary between the zones, so that the Ta-rich phase could be considered as an overgrowth. Moreover, these rims are partially dissolved (Fig. 3). Oscillatory zoning also occurs, with multiple bright Ta-rich, and dark Nb-rich bands. Reverse zoning, where the core is Ta-rich and rims are Nb-rich (Lahti, 1987) is quite abundant. This zoning is relatively common in Nb-Ta-group minerals (Belkasmi *et al*., 2000; Neiva *et al*., 2008; Abdalla *et al*., 1998; Anderson *et al*., 2013). Irregular patchy zoning is also present, which is usual in CGM from rare-metal granites (Tadesse and Zerihun, 1996) and pegmatitic occurrences (Alfonso *et al*., 1995; Tindle and Breaks, 2000; Uher *et al*., 2007). In other cases these minerals exhibit convoluted zoning or are homogeneous. Zoning often shows a complex combination of different types, such as oscillatory and patchy. Patchy zonation has been interpreted as evidence for replacement involving partial resorption of an early columbite and the generation of a more Ta-rich composition usually along the margins of crystals (Abdalla *et al*., 1998).

Many of the CGM exhibit corrosion or dissolution with sponge-like textures that affect the columbite rims, and the tantalite rims in particular. This corrosion destroys columbite that is replaced by tantalite. Similar dissolution textures are evident in other Nb-Ta minerals from pegmatites (e.g. Wise and Brown, 2010; Dill *et al*., 2015).

The chemical composition of 490 points of CGM from ~130 crystals was determined (Table 1). Atomic compositions and ratios were calculated and plotted on the columbite quadrilateral, where most compositions are

TABLE 1. Representative chemical composition of the Penouta leucogranite and the associated greisen.

	Leucogranite		Greisen (outcrop)		Greisen (Drill Hole 3)										
Oxides (wt.%)	P14	P-Tot	P-22	P-24	D02630	D02630	D02630	D02630	D02630	D02630	D02630	D02630	D02630	D02630	D02630
SiO_2 (wt.%)	70.38	74.9	67.18	67.39	64.8	64.2	57	61.9	61.7	61.5	61.2	57	57.7	61.5	57.8
Al_2O_3	17.95	15.3	18.52	18.29	19.25	19.75	24.1	21.6	20.1	21.8	21	24.6	23.2	20.4	23.3
TiO_2	b.d.l.	b.d.l.	0.58	0.55	0.33	0.37	0.42	0.42	0.43	0.54	0.39	0.38	0.5	0.51	0.52
FeO	0.48	0.67	3.91	3.91	2.87	2.99	2.96	3.38	3.45	3.88	3.11	3.33	4.05	3.78	4.12
MnO	0.03	0.05	0.12	0.20	0.27	0.24	0.26	0.29	0.52	0.22	0.24	0.28	0.28	0.29	0.26
CaO	0.11	0.15	0.03	0.04	b.d.l.	b.d.l.	b.d.l.	b.d.l.	0.01	b.d.l.	b.d.l.	b.d.l.	b.d.l.	0.13	0.62
MgO	0.03	0.04	0.46	0.56	0.89	0.92	0.98	1.06	1.08	1.25	0.99	1	1.2	1.29	1.34
Na_2O	5.59	5.14	b.d.l.	b.d.l.	0.15	0.15	0.17	0.19	0.17	0.16	0.18	0.2	0.18	0.17	0.71
K_2O	4.23	3.18	3.25	4.51	6.57	6.41	6.9	7.11	6.81	6.79	7.17	7.84	7.2	6.98	7.34
P_2O_5	0.02	0.03	0.08	0.09	0.05	0.04	0.06	0.04	0.04	0.06	0.02	0.04	0.05	0.12	0.32
L.O.I.	n.d.	n.d.	n.d.	n.d.	3.3	3.71	5.09	3.78	3.8	4.34	3.67	4.43	4.69	3.98	3.95
Total	98.82	99.46	94.14	95.55	98.9	99.2	98.37	100.2	98.6	101.1	98.4	99.56	99.6	99.67	100.9
Nb (ppm)	64	81	15	18	37.2	41.7	65.3	55.2	37.6	44.2	43.9	57.5	48.3	38.7	52.7
Ta	140	103	10	16	32.6	36.3	85.5	59.4	27.5	40.9	31.9	46.6	28.5	30.7	52.7
Sn	569	383	4,5	11,6	1000	1090	2870	1610	662	1440	626	1900	483	672	1630
W	105	35	7,7	275	14	28	27	32	30	28	23	27	26	25	21
U	1.6	2.5	4.6	5.2	1.62	2.5	2.12	4.48	3.55	3.63	3.64	1.92	2.87	4.02	4.02
Th	3.3	2.4	12.8	12.8	7.35	7.2	8.19	10.75	8.5	8.05	10.85	8.74	7.46	10.05	11.75
Li	129	130	493	614	n.d.	n.d.	n.d.	n.d.	n.d.	n.d.	n.d.	n.d.	n.d.	n.d.	n.d.
Rb	1070	966	696	1160	1345	2320	2380	2340	2630	2390	2310	2660	2730	2730	2300
Cs	43.4	64	29.7	53	67.7	128.5	129	116	133.5	120	145.5	160	175	180	144
Ba	87	16	500	682	513	578	536	605	544	669	572	534	506	659	603
Be	125	-	8	10	n.d.	n.d.	n.d.	n.d.	n.d.	n.d.	n.d.	n.d.	n.d.	n.d.	n.d.
Mg/Li	1.6	1.9	5.7	5.5	-	-	-	-	-	-	-	-	-	-	-
A/(CNK)	1.8	1.8	2.2	2.1	2.61	2.75	3.11	2.70	2.62	2.86	2.60	2.79	2.87	2.53	2.27
K/Rb	32.0	26.6	37.8	31.4	40.1	22.7	23.8	24.9	21.2	23.3	25.5	24.2	21.6	20.9	26.2
K/Cs	788	402	885	688	796	409	439	503	418	464	404	402	337	318	418
Nb/Ta	0.5	0.8	1.5	1.1	1.14	1.15	0.76	0.93	1.37	1.08	1.38	1.23	1.69	1.26	1.00

b.d.l.: below detection limit; n.d.: not determined; A/(CNK): molar $Al_2O_3/(CaO + Na_2O + K_2O)$.

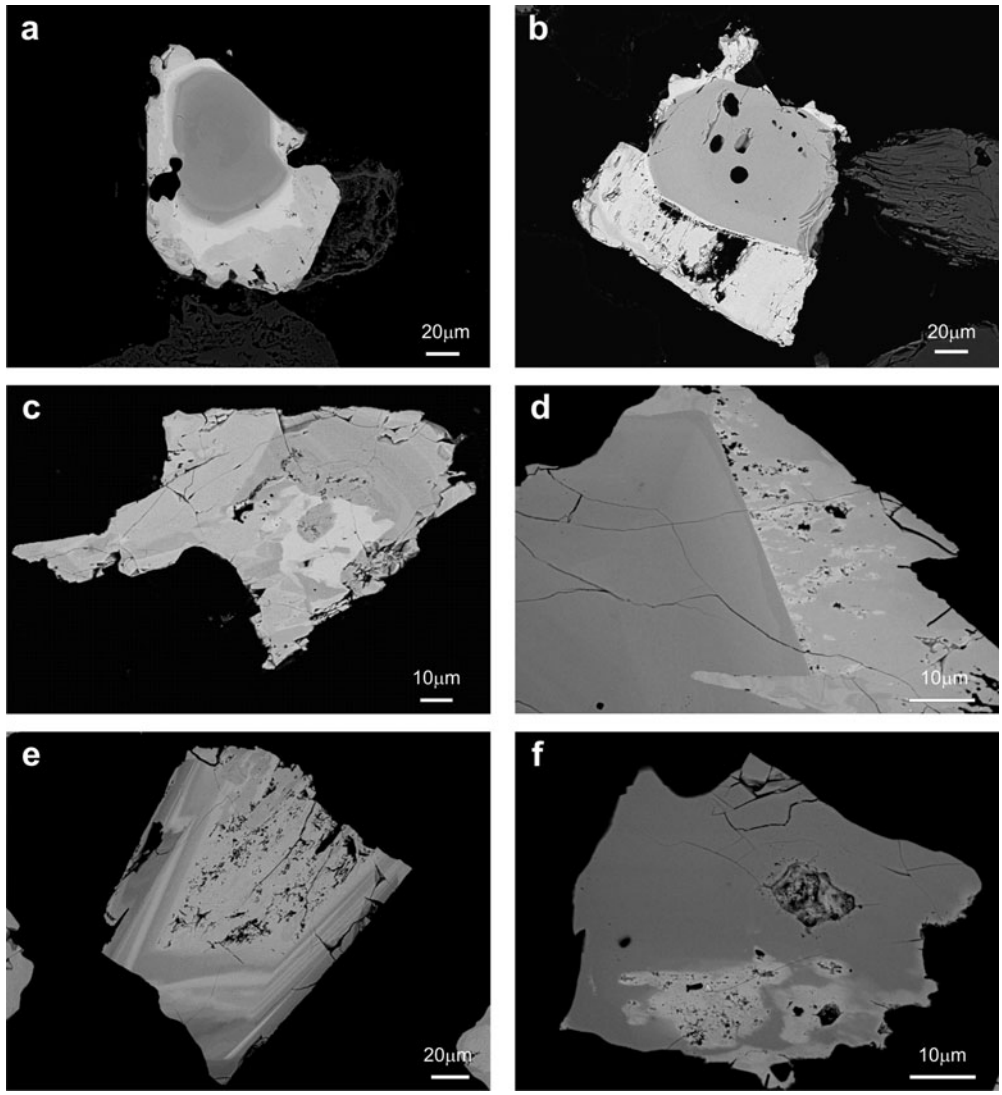

FIG. 3. Back-scattered SEM images of CGM from the Penouta leucogranite: (*a*) typical zoned crystal with a Nb-rich core (dark) and a Ta-rich rim (bright); (*b*) columbite crystal with an overgrowth of tantalite; (*c*) columbite-tantalite with patchy zoning (*d*) Columbite with a rim of tantalite; (*e*) reverse oscillatory zoning, with a dissolution texture in the innermost Ta-rich phase; (*f*) columbite with a Ta replacement.

manganotantalite and manganocolumbite (Fig. 5). The Mn/(Mn + Fe) ratio varies between 0.33 and 0.97 and the Ta/(Ta + Nb) ratio between 0.07 and 0.93. These values are typical of highly evolved magmatic systems. Two clusters can be observed, both at Mn/(Mn + Fe) = 0.8, one at Ta/(Ta + Nb) = 0.1–0.2 and the other at Ta/(Ta + Nb) = 0.5–0.8, that correspond to the cores and rims of the crystals, respectively. The TiO_2 content is <0.5 wt.%, except in one crystal, where TiO_2 ranges from 2.17 to 2.76 wt.%. This crystal is also relatively Y-rich, varying from 1.09 to 1.30 wt.% Y_2O_3.

Columbite-group minerals are relatively poor in minor elements (Table 2). Microprobe analyses reveal variable contents of Sn and W, usually <1 wt. %, although they can occasionally reach 2.71 and 2.54 wt.%, respectively. Ca, Y, U and Th are negligible. The ZrO_2 content is up to 0.28 wt.%

FIG. 4. MLA map from a concentrate of Nb-Ta oxide minerals from Penouta. The common texture of CGM, i.e. a Nb-rich core and a Ta-rich rim, is observed and the association of columbite–tantalite with quartz and muscovite is noted.

and HfO_2 up to 0.16 wt.%. Sb and Bi are below the detection limits of the EMPA.

Ferrotapiolite

Tapiolite is rare; only one crystal of 10 µm was detected as an inclusion in cassiterite. Its chemical composition shows a Ta/(Ta + Nb) ratio of 0.89 and Mn/(Mn + Fe) ratio of 0.11 (Table 2).

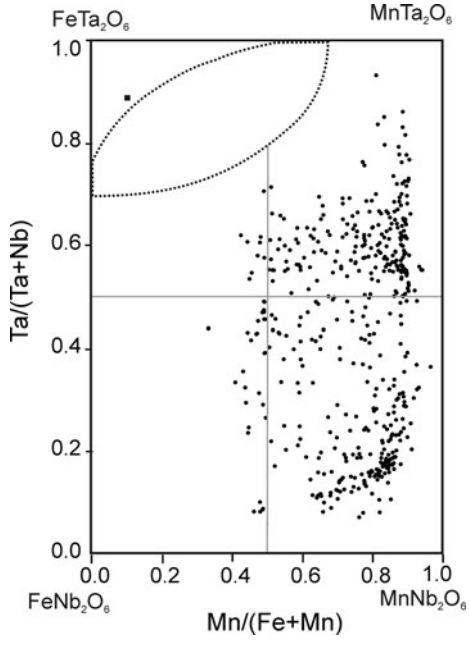

FIG. 5. Composition of the CGM (dots) and tapiolite (square) from the Penouta leucogranite in the columbite quadrilateral (atomic ratios).

Microlite

Primary euhedral microlite crystals are rare and only a few micrometres in size. This mineral usually occurs as a late phase associated with CGM. In most cases microlite is enclosed in tantalite and cassiterite. According to the MLA data only 12 wt.% of the microlite crystals are 'free', whereas 24 wt.% were in contact with tantalite and 14 wt.% with cassiterite. Representative compositions of microlite are given in Table 3. Microlite is always Ta-rich, with Ta/(Ta + Nb) values varying between 0.91 and 0.99. Its composition ranges from 64.00 to 80.27 wt.% of Ta_2O_5 and 2.36 to 16.92 wt.% of Nb_2O_5; TiO_2 reaches 0.25 wt.% and SnO_2 varies between 0.38 and 3.44 wt.% . The occupation of the *A* site varies considerably; Ca is the most abundant cation, up to 11.89 wt.%, but U and Pb can also be significant, with up to 6.01 and 8.46 wt.%, respectively. Plumbomicrolite occurs as a thin rim around microlite (Fig. 6). Na_2O contents reach 5.86 wt.%, whereas SnO reaches 3 wt.%. Fluorine is present in small amounts, up to 0.17 wt.%. Antimony and Bi were not detected.

Wodginite

Wodginite occurs associated with cassiterite and tantalite (Fig. 6) as late replacements or inclusions. The differentiation between ixiolite and wodginite is based on the structure, but stoichiometric criteria

TABLE 2. Representative chemical composition of CGM and tapiolite from the Penouta leucogranite.

Oxides (wt.%)	P31 MT	P42 FT	P91 MT	P94 MT	P112 MT	P117 MT	P119 MC	P120 MC	P143 Tp
WO_3	0.31	0.32	0.26	0.15	0.41	0.24	0.35	0.21	0.41
Ta_2O_5	67.82	66.47	64.64	52.20	55.08	65.41	44.92	19.28	76.42
Nb_2O_5	15.47	16.68	18.54	30.04	27.61	17.94	36.57	60.71	5.77
TiO_2	0.00	0.00	0.05	0.00	0.23	0.07	0.06	0.05	0.11
UO_2	0.02	0.35	0.10	0.09	0.00	0.29	0.30	0.08	0.16
ThO_2	0.00	0.00	0.00	0.03	0.00	0.00	0.00	0.00	0.00
Sc_2O_3	0.20	0.24	0.22	0.19	0.22	0.22	0.17	0.04	0.24
ZrO_2	0.07	0.28	0.07	0.04	0.04	0.09	0.02	0.00	0.07
HfO_2	0.04	0.16	0.03	0.05	0.00	0.00	0.00	0.00	0.04
SnO_2	0.76	0.27	0.02	0.07	0.04	0.16	0.20	0.08	1.18
Fe_2O_3	0.38	0.43	1.29	0.95	0.37	0.74	0.21	0.37	0.70
FeO	1.48	7.92	4.72	0.95	3.35	2.81	7.97	3.52	12.36
MnO	13.30	7.09	10.04	14.96	12.75	12.13	9.02	15.70	1.29
CaO	0.03	0.00	0.01	0.00	0.01	0.01	0.00	0.00	0.00
PbO	0.12	0.00	0.00	0.00	0.00	0.03	0.00	0.00	0.05
Total	99.99	100.22	100.00	99.73	100.11	100.14	99.78	100.04	98.80
				Atomic contents					
W^{6+}	0.025	0.026	0.020	0.011	0.031	0.019	0.025	0.013	0.009
Ta^{5+}	5.685	5.528	5.304	4.029	4.295	5.393	3.357	1.274	1.715
Nb^{5+}	2.156	2.306	2.529	3.855	3.579	2.459	4.544	6.668	0.215
Ti^{2+}	0.000	0.000	0.012	0.000	0.050	0.016	0.012	0.009	0.007
U^{4+}	0.001	0.024	0.007	0.006	0.000	0.020	0.018	0.004	0.003
Th^{4+}	0.000	0.000	0.000	0.002	0.000	0.000	0.000	0.000	0.000
Sc^{3+}	0.054	0.063	0.057	0.047	0.054	0.057	0.040	0.009	0.017
Zr^{4+}	0.010	0.042	0.010	0.006	0.006	0.013	0.003	0.000	0.003
Hf^{4+}	0.004	0.014	0.003	0.004	0.000	0.000	0.000	0.000	0.001
Sn^{4+}	0.104	0.037	0.003	0.009	0.005	0.021	0.024	0.008	0.043
Fe^{3+}	0.088	0.099	0.293	0.203	0.080	0.169	0.043	0.068	0.043
Fe^{2+}	0.382	2.025	1.191	0.231	0.803	0.713	1.833	0.715	0.853
Mn^{2+}	3.472	1.836	2.566	3.597	3.096	3.115	2.100	3.231	0.090
Ca^{2+}	0.009	0.000	0.004	0.000	0.001	0.002	0.001	0.000	0.000
Pb^{2+}	0.010	0.000	0.000	0.000	0.000	0.002	0.000	0.000	0.001
Σcations	12.000	12.000	12.000	12.000	12.000	12.000	12.000	12.000	3.000
Ta/(Ta + Nb)	0.725	0.706	0.677	0.511	0.545	0.687	0.425	0.160	0.888
Mn/(Fe + Mn)	0.881	0.464	0.633	0.892	0.778	0.779	0.528	0.805	0.091

MT – manganotantalite; FT – ferrotantalite; MC – manganocolumbite; Tp – tapiolite.

TABLE 3. Representative chemical composition (wt.%) of microlite from the Penouta leucogranite.

Sample	P034	P037	P132	P057	P202	P2036	P2037	P2026
WO_3	0.33	0.22	0.43	0.40	0.25	0.25	0.17	0.35
Ta_2O_5	75.00	75.15	74.63	73.78	71.72	71.02	71.30	70.41
Nb_2O_5	3.10	2.92	2.95	3.36	5.20	5.50	5.34	4.94
TiO_2	0.06	0.07	0.08	0.10	0.25	0.14	0.17	0.12
UO_2	1.48	1.31	1.71	6.07	1.51	0.26	0.19	1.49
ThO_2	0.00	0.00	0.00	0.00	0.00	0.47	0.39	0.05
Sc_2O_3	n.d.	n.d.	n.d.	n.d.	n.d.	0.13	0.15	0.25
ZrO_2	n.d.	n.d.	n.d.	n.d.	n.d.	0.00	0.15	0.14
HfO_2	n.d.	n.d.	n.d.	n.d.	n.d.	0.00	0.00	0.07
CaO	10.87	10.92	10.53	9.56	0.88	11.36	11.51	11.03
Y_2O_3	0.12	0.00	0.05	0.16	0.00	0.00	0.00	0.00
MnO	0.16	0.09	0.28	0.41	0.55	0.05	0.10	0.13
FeO	0.24	0.68	1.43	0.25	0.71	0.09	0.10	0.11
SnO_2	1.91	1.88	1.72	0.93	2.67	2.99	2.61	2.56
PbO	0.18	0.15	0.06	0.26	8.46	0.09	0.17	0.04
Na_2O	5.92	5.72	5.74	4.40	0.03	4.94	5.11	4.63
F	n.d.	n.d.	n.d.	n.d.	0.07	0.13	0.15	0.12
OH	0.78	0.78	0.60	1.01	4.76	0.85	0.08	0.85
O = F					–0.97	–0.94	–0.94	–0.95
Total	100.14	99.88	100.21	100.69	96.08	97.34	96.75	96.33
			Atomic contents					
Ca^{2+}	1.062	1.070	1.035	0.941	0.085	1.108	1.119	1.092
Y^{3+}	0.006	0.000	0.002	0.008	0.000	0.000	0.000	0.000
U^{4+}	0.030	0.027	0.035	0.124	0.030	0.005	0.004	0.031
Th^{4+}	0.000	0.000	0.000	0.000	0.000	0.010	0.008	0.001
Pb^{2+}	0.004	0.004	0.002	0.006	0.206	0.002	0.004	0.001
Sn^{2+}	0.070	0.068	0.063	0.038	0.108	0.122	0.106	0.105
Na^{+}	1.047	1.014	1.021	0.784	0.005	0.872	0.899	0.829
Fe^{2+}	0.018	0.052	0.110	0.019	0.054	0.007	0.008	0.009
Mn^{2+}	0.012	0.007	0.022	0.032	0.042	0.004	0.008	0.010
Σ*A* site	2.250	2.242	2.289	1.953	0.530	2.129	2.155	2.08
W	0.008	0.005	0.010	0.009	0.006	0.006	0.004	0.008
Nb	0.128	0.121	0.122	0.140	0.213	0.226	0.219	0.206
Ta	1.861	1.869	1.862	1.844	1.765	1.758	1.759	1.769
Ti	0.004	0.005	0.006	0.007	0.017	0.010	0.011	0.008

(continued)

TABLE 3. (*contd.*)

Sample	P034	P037	P132	P057	P202	P2036	P2037	P2026
Zr	-	-	-	-	0.000	0.000	0.007	0.006
Hf	-	-	-	-	0.000	0.000	0.000	0.002
Σ*B* site	2.000	2.000	2.000	2.000	2.000	2.000	2.000	2.000
F^-	-	-	-	-	0.020	0.038	0.042	0.035
OH^-	0.477	0.476	0.367	0.620	2.875	0.517	0.503	0.524
Oxygens	6.523	6.524	6.633	6.380	4.105	6.445	6.455	6.441
Σanions	7.000	7.000	7.000	7.000	7.000	7.000	7.000	7.000
Ta/(Ta + Nb)	0.94	0.94	0.94	0.93	0.89	0.89	0.89	0.90

can also be used (Wise *et al*., 1998). As shown in Table 4, most analyses fit well with the formula of wodginite. The *B* and *C* sites are completed and only *A*-site values are slightly less than that of the ideal formula (Table 4). This may be due to the presence of Li or vacancies (Ercit *et al*., 1992*a*).

According to the classification criteria of Ercit *et al*. (1992*b*), most of the wodginite group minerals analysed are wodginite and only some compositions are of ferrowodginite. Ta_2O_5 ranges from 48.36 to 65.35 wt.%., SnO_2 from 14.63 to 19.37, MnO from 4.36 to 10.91. W is usually <1 wt.% but can reach 4.19 wt.%. The W content is correlated with the total Fe (Fig. 7). Hf and Zr are present in relatively large amounts, up to 1.34 wt.% of HfO_2 and 1.29 wt.% of ZrO_2. The average Zr/Hf ratio is ~0.7. Such large amounts have only been reported by Černý *et al*. (2007) for granitic pegmatites. In contrast with Černý *et al*. (2007) there is a slight correlation here between the Ta/(Ta + Nb) and Hf/(Hf + Zr) (Fig. 8).

Cassiterite

Cassiterite is the main oxide mineral in the Penouta leucogranite. It occurs as subhedral to euhedral crystals usually up to 200 μm long. Under BSE, cassiterite seems to be homogeneous in appearance; the chemical composition varies, however. Two generations can be recognized. The first generation consists of homogeneous crystals of nearly pure composition, whereas, in the second generation, Ta can reach 8.51 wt.% Ta_2O_5, and the Nb content is up to 1.94 wt.% Nb_2O_5. As usual in greisens and veins from granites, Fe is dominant over Mn (Černý and Ercit, 1989), reaching 1.45 wt.% and 0.20 wt.%, respectively. In granitic pegmatites the presence of Nb and Ta within cassiterite is attributed to the typical substitution scheme $(Fe,Mn)^{2+} + 2(Nb,Ta)^{5+} \leftrightarrow 3(Sn,Ti)^{4+}$, or tapiolite substitution (Černý *et al*., 1985), in which case the (Fe + Mn)/(Nb + Ta) ratio is in a 1 : 2 proportion (Černý *et al*., 2004). Most analyses from the Penouta cassiterite show the 1 : 2 ratio to be attributed to the tapiolite substitution (Fig. 9*a*).

The cassiterite grains typically contain inclusions of Nb-Ta-rich minerals (Spilde and Shearer, 1992). Similarly, wodginite inclusions have also been found in other deposits (Masau *et al*., 2000; Černý *et al*., 2007; Rao *et al*., 2009). Masau *et al*. (2000) described Hf-Zr-rich wodginite formed by exsolution from cassiterite, which was favoured by its high Zr and Hf contents. In the present study the

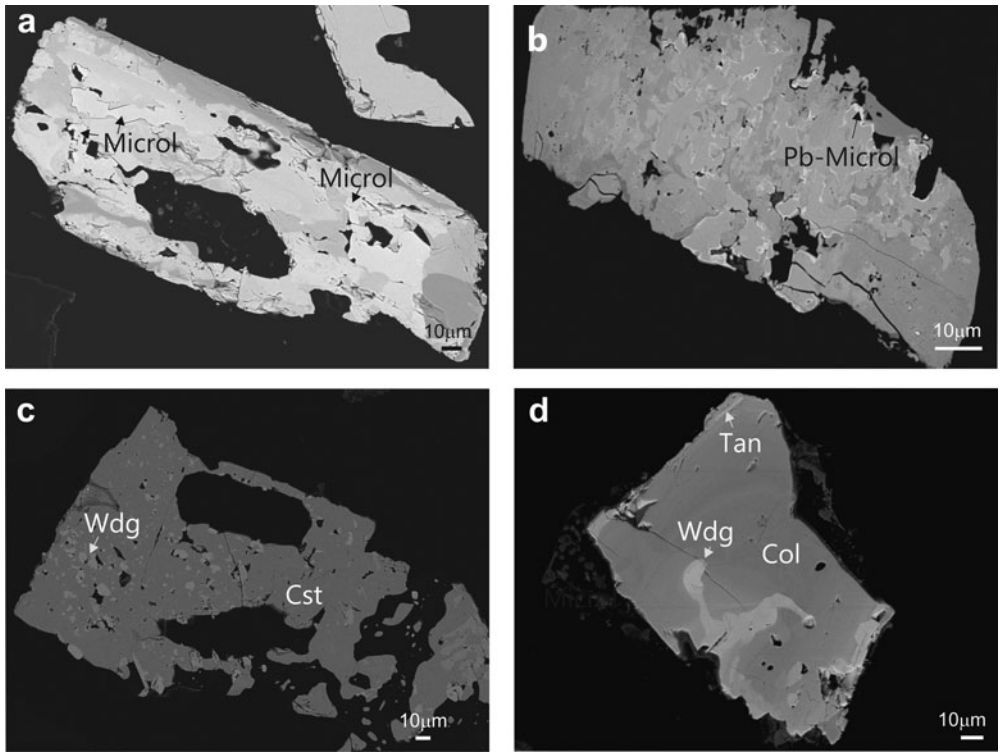

FIG. 6. Back-scattered SEM images of Na-Ta oxides from the Penouta leucogranite: (*a*) columbite–tantalite crystal with microlite (Microl) enclosed (bright); (*b*) microlite replacement of columbite with bright rims composed of plumbomicrolite (Pb-Microl); (*c*) wodginite (Wdg) inclusions in cassiterite (Cst); (*d*) wodginite replacement in CGM, with a Nb-rich core (dark), and a Ta-rich rim (Tan) (bright).

Hf and Zr contents are relatively high in wodginite, suggesting a possible similar origin. However, inclusions of CGM in cassiterite constitute discrete grains probably trapped when cassiterite formed after CGM, as in other occurrences (Martins *et al*., 2011).

Discussion

Two aspects cause a great deal of controversy in the genesis of Nb-Ta deposits, both pegmatites and granites: (1) the rare-metal enrichment of the melts; and (2) the fractionation between Nb and Ta, with special emphasis on the magmatic *vs.* hydrothermal enrichment of the late Ta-rich phases.

In the genesis of the of the Penouta deposit, three stages can be distinguished: (1) a primary magmatic stage; (2) a late metasomatic stage with albitization and muscovitization; and (3) an epigenetic or supergene stage. The existence of these stages has been supported by field and geochemical evidence and also by a fluid-inclusion study carried out by Mangas and Arribas (1991).

Magmatic crystallization of CGM and related textures

Whole-rock Ta distribution in the Penouta granite exhibits a progressive Ta enrichment upwards in the granite sheet. Evidence of the saturation of columbite-tantalite was not attained; if it had been, a depletion in Ta contents would have occurred once this mineral phase reached its saturation, as CGM contain Ta, an essential structural constituent (ESC) in these mineral phases (López Moro *et al*., 2017). There is petrographical evidence, however, of the occurrence of CGM from the bottom to the top of the Penouta granite body and an external origin (assimilated or residual minerals) can be ruled

TABLE 4. Representative chemical composition (wt.%) of wodginite from the Penouta leucogranite.

	PW1	PW2	PW3	PW4	PW5	PW6
WO_3	0.49	0.36	0.39	0.35	0.17	0.21
Ta_2O_5	61.85	62.02	61.35	63.52	63.27	63.69
Nb_2O_5	7.51	7.05	7.40	6.20	7.23	6.10
TiO_2	0.11	0.09	0.21	0.08	0.05	0.08
UO_2	0.10	0.00	0.00	0.207	0.00	0.05
ThO_2	0.00	0.00	0.00	0.00	0.00	0.05
Sc_2O_3	0.21	0.08	0.14	0.14	0.08	0.11
ZrO_2	0.37	0.55	0.40	0.54	0.44	0.46
HfO_2	0.67	0.77	0.46	1.00	0.63	0.47
CaO	0.04	0.06	0.05	0.04	0.06	0.06
MnO	5.17	5.63	5.07	9.03	8.18	6.60
FeO	6.1	5.65	6.31	1.87	3.05	4.53
SnO_2	14.83	15.31	16.26	14.36	15	15.32
Fe_2O_3	1.53	1.40	1.17	1.77	1.57	1.44
PbO	0.13	0.03	0.00	0.00	0.20	0.15
Total	99.10	98.99	99.21	99.11	99.93	99.33
			Atomic contents			
Mn^{2+}	1.828	1.996	1.785	3.239	2.878	2.349
Fe^{2+}	2.129	1.984	2.193	0.662	1.060	1.591
Ca^{2+}	0.018	0.016	0.020	0.018	0.026	0.029
U^{4+}	0.009	0.000	0.000	0.020	0.000	0.004
Th^{4+}	0.000	0.000	0.000	0.000	0.000	0.005
Pb^{2+}	0.014	0.003	0.000	0.000	0.022	0.017
Σ*A* site	3.998	3.999	3.999	3.938	3.986	3.995
Sn^{4+}	2.761	2.874	3.015	2.712	2.779	2.871
Ti^{4+}	0.035	0.029	0.064	0.026	0.016	0.024
Fe^{3+}	0.481	0.442	0.366	0.437	0.491	0.455
Ta^{5+}	0.491	0.422	0.368	0.541	0.523	0.457
Sc^{3+}	0.078	0.029	0.050	0.050	0.028	0.042
Hf^{4+}	0.080	0.092	0.055	0.121	0.074	0.057
Zr^{4+}	0.075	0.111	0.082	0.112	0.090	0.095
Σ*B* site	4.000	4.000	4.000	4.000	4.000	4.000
Ta^{5+}	6.530	6.758	6.568	6.774	6.623	6.820
Nb^{5+}	1.417	1.204	1.391	1.187	1.358	1.159
W^{6+}	0.053	0.039	0.043	0.038	0.019	0.023
Σ*C* site	8.000	8.001	8.002	7.999	7.999	8.002
Σcations	15.998	16.001	16.001	15.937	15.986	15.997

out. Both observations suggest that CGM grew within trapped intercumulus melt, where the crystallization of major rock-forming minerals incompatible with Ta and Nb (e.g. quartz, alkali feldspar and albite) increased the concentration of Ta and Nb in the shrinking residual melt until saturation occurred. Crystallization of CGM in the Penouta granite seems to have occurred far from the liquidus of the parental magma, but related to local saturation. In a scenario of local saturation, Nb tends to crystallize prior to Ta due to the lower solubility of Nb in peraluminous melts (Keppler, 1993; Linnen and Keppler, 1997; Linnen, 1998; Stepanov *et al*., 2014), resulting in a normal zoning that is very common in columbite–tantalites from the Penouta leucogranite (e.g. Fig. 3). CGM from the Penouta leucogranite also exhibit often-complex zoning patterns (e.g. oscillatory zoning), that could be explained in a magmatic scenario. Extrinsic mechanisms, such as temperature or water-pressure changes (Shore and Fowler, 1996) or intrinsic mechanisms, such as non-equilibrium concentration gradients (Bacon, 1989) have been proposed to explain such rhythmic zoning.

The primary character of CGM is also in line with their core Ta/Nb variation observed from

TABLE 5. Representative chemical composition (wt.%) of cassiterite from the Penouta leucogranite.

	PC12	PC17	PC105	PC110	PC211	PC013	PC086	PC213
WO_3	0.00	0.11	0.00	0.00	0.00	0.05	0.00	0.00
Ta_2O_5	0.56	6.27	2.98	3.15	0.12	2.59	1.38	5.41
Nb_2O_5	0.10	0.87	0.53	0.50	0.00	0.37	0.35	0.46
TiO_2	0.00	0.00	0.02	0.00	0.00	0.41	0.01	0.04
SnO_2	99.29	91.53	96.02	96.14	99.38	95.44	97.26	92.18
FeO	0.08	1.02	0.81	0.65	0.03	0.54	0.81	0.89
MnO	0.03	0.26	0.12	0.12	0.00	0.04	0.00	0.24
CaO	0.00	0.00	0.30	0.32	0.32	0.30	0.31	0.32
Y_2O_3	0.00	0.16	0.01	0.02	0.00	0.00	0.09	0.00
PbO	n.d.	n.d.	0.04	0.01	0.08	0.00	0.18	0.11
Total	100.05	100.21	100.83	100.92	99.93	99.75	100.40	99.66
				Atomic contents				
W^{6+}	0.000	0.001	0.000	0.000	0.000	0.001	0.000	0.000
Ta^{5+}	0.008	0.086	0.040	0.043	0.002	0.035	0.019	0.074
Nb^{5+}	0.002	0.020	0.012	0.011	0.000	0.008	0.008	0.011
Ti^{2+}	0.000	0.000	0.001	0.000	0.000	0.015	0.000	0.001
Sn^{4+}	1.986	1.836	1.906	1.908	1.988	1.908	1.938	1.859
Fe^{2+}	0.004	0.043	0.034	0.027	0.001	0.023	0.034	0.038
Mn^{2+}	0.001	0.011	0.005	0.005	0.000	0.002	0.000	0.010
Ca^{2+}	0.000	0.000	0.016	0.017	0.017	0.016	0.017	0.017
Y^{3+}	0.000	0.004	0.000	0.001	0.000	0.000	0.002	0.000
Pb^{2+}	-	-	0.001	0.000	0.001	0.000	0.002	0.002
Σcations	2.000	2.001	2.015	2.011	2.009	2.009	2.020	2.012

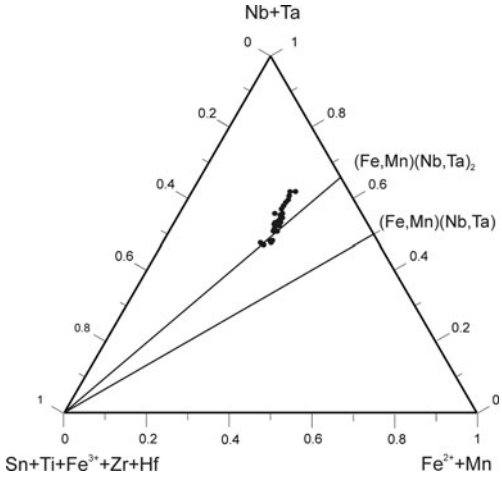

FIG. 7. Compositions of wodginite-group minerals in the (Nb,Ta)–(Sn,Ti,Fe^{3+})–(Fe,Mn) diagram (atomic ratios).

bottom to top in the granite (Fig. 10). Because CGM phases were saturated only locally in a trapped melt, the Ta/Nb variation of cores has to be a consequence of the fractionation process of the liquidus mineral phases (e.g. quartz, alkali feldspar, albite, muscovite and garnet). The distribution coefficients of these liquidus minerals for Ta and Nb are typically incompatible except for muscovite, which would fractionate Nb relative to Ta (D_{Nb} = 3.5; D_{Ta} = 0.4; Raimbault and Burnol, 1998), contributing to the increase in the Ta/Nb ratio as the melt evolves. Whole-rock ratio variations in Ta/Nb from the Penouta granite have been modelled recently, taking into account, among others factors, muscovite as a fractionated mineral phase, resulting in a good match between modelled and real melt

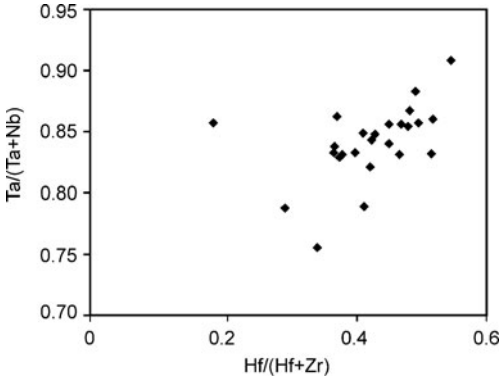

FIG. 8. Correlation between the Ta/(Ta + Nb) and Hf/(Hf + Zr) in wodginite from Penouta.

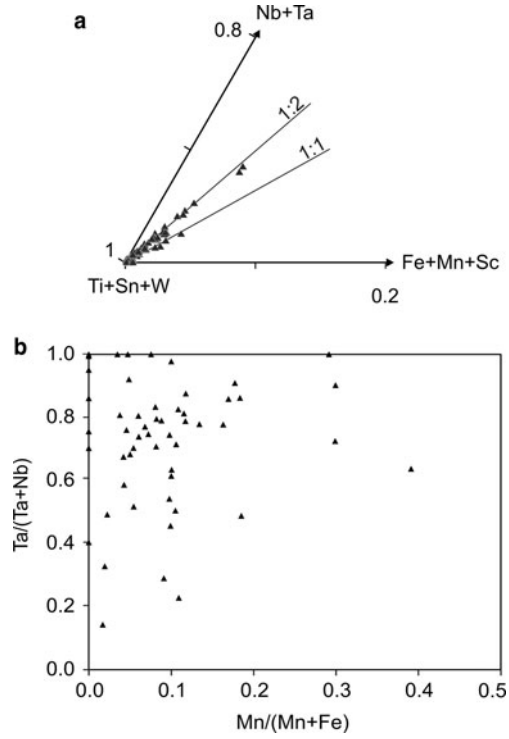

FIG. 9. Cassiterite composition from the Penouta leucogranite: (*a*) plot in the (Ti + Sn + W)–(Fe + Mn + Sc)–(Nb + Ta) triangle; (*b*) in the columbite quadrilateral (atomic ratios).

evolution (López Moro *et al.*, 2017). Consequently, the involvement of muscovite as a fractionated liquidus mineral phase could explain core Ta/Nb variations of CGM from bottom to top in the Penouta granite and the magmatic origin of normal zoning of CGM.

Overprints on CGM

One of the most striking features of back-scattering images of CGM is the occurrence of a large number of micro holes, frequently grouped, and within areas with a marked Nb depletion and Ta enrichment relative to surrounding blackish areas of the crystal (Fig. 3). These textures have been cited in many other occurrences (e.g. Galliski *et al.*, 2008; Wise and Brown, 2010; Zhu *et al.*, 2015), are known as 'sponge-like' textures and resemble textures related to overprinting processes in an environment enriched in fluids during their formation. However, the origin of this fluid is an open issue but could be linked to the evolution of the

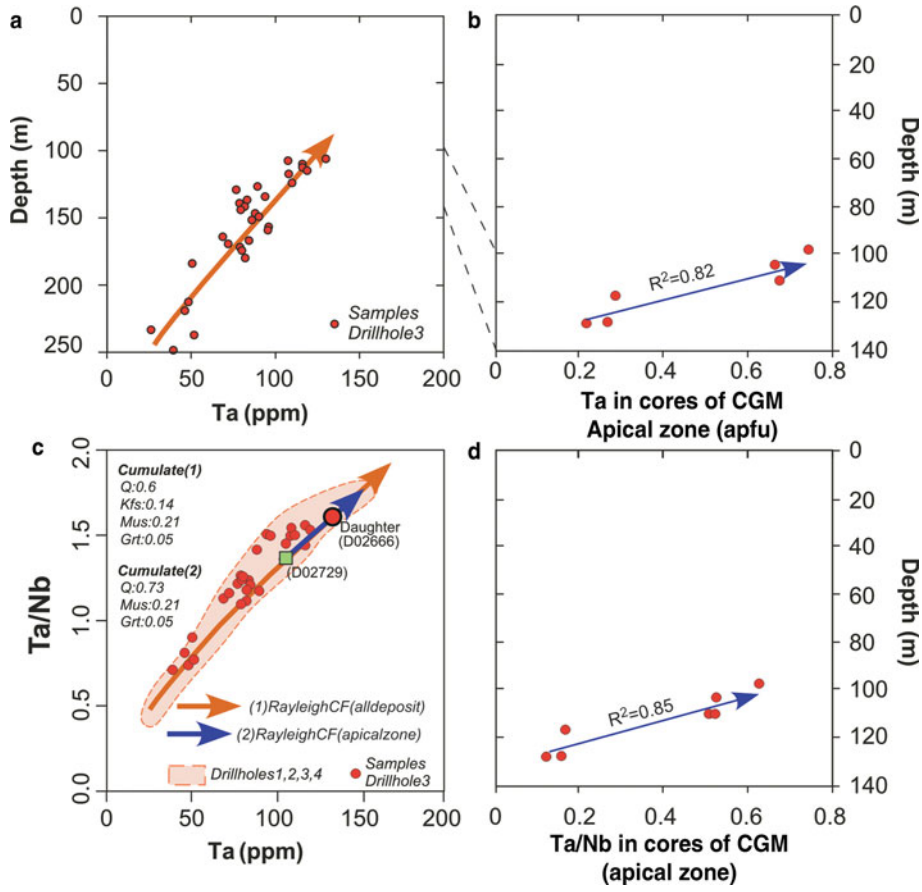

FIG. 10. Variation with depth in the Penouta deposit: (*a*) Ta content in granite; (*b*) Ta content in cores of CGM; (*c*) Ta *vs.* Ta/Nb; and (*d*) Ta/Nb variation observed from bottom to top in the granite.

magma itself or to processes unrelated to the magmatic process.

(1) Processes related to the evolution of the melt

Experimental and fluid/melt inclusion studies have demonstrated that during the last stage of magmatic crystallization, an exsolution process can occur, resulting in up to three products, namely, a silicate melt, vapour and a hydrosaline phase, the latter being described either as a fluid (Roedder, 1992; Kamenetsky *et al*., 2004; Alfonso and Melgarejo, 2008; Tartèse and Boulvais, 2010; Chicharro *et al*., 2015; Webster *et al*., 2015; Assadzadeh *et al*., 2017) or as a melt (Badanina *et al*., 2004; Veksler, 2004; Thomas and Davidson, 2013; Huang *et al*., 2015).

The hydrosaline phase was defined as a melt rich in fluxing elements such as Cl, Li, B and/or F; which are fluxing elements with low solubility in aluminosilicate melt and which fractionate to the hydrosaline phase, causing its low viscosity (Veksler, 2004; Linnen and Cuney, 2005). In such conditions this fluid/melt could easily move and produce metasomatism during its interaction with the early formed minerals and consequently the formation of the sponge-like textures. The existence of an exsolution process resulting in a hydrosaline phase can be checked by the mineralogical and geochemical fingerprints left by this process.

(a) The role played by B-enriched hydrosaline fluids

A B-enriched hydrosaline fluid can be practically ruled out in the Penouta deposit, because

tourmaline is a very accessory mineral and also by the deposit type itself. Boron-bearing melts provide evidence of explosive processes such as the formation of breccia pipes and stockworks (Pollard *et al*., 1987), whereas in the Penouta leucogranite the mineralization is disseminated, indicating a passive crystallization of the magma.

(b) The role played by F-enriched hydrosaline fluids

The occurrence of a F-enriched hydrosaline fluid/melt in the apical zone, where the sponge-like textures of CGM occur, should trigger the following mineralogical and geochemical fingerprints according to the distribution coefficients between silicate and a fluoride-enriched hydrosaline melt compiled by Veksler (2004): (1) Na would be fractionated into the hydrosaline melt and K would remain in the aluminosilicate melt; (2) Ta and Hf appear to be much less compatible with F hydrosaline melts than Nb and Zr, resulting in lower Zr/Hf and Nb/Ta ratios in the residual silicate melt and the opposite in the hydrosaline melt; (3) Y and *REE* are highly fractionated in the F hydrosaline fluid/melt, resulting in a depleted aluminosilicate melt in these elements.

The evolution of Zr/Hf and Nb/Ta ratios, together with Y and *REE* depletion in the silica melt and the Na enrichment upwards in the granite are consistent with whole-rock evolutions observed in the Penouta granite on a deposit scale (see López Moro *et al*., 2017). However, most of these geochemical constraints can also be explained in terms of fractional crystallization involving quartz, muscovite, alkali feldspar, zircon, monazite and xenotime as fractionated mineral phases (López Moro *et al*., 2017). A similar conclusion can be drawn for the albite enrichment of the apical zone, since a change in the ternary cotectic in the system Qz–Ab–Or can be yielded as a consequence of F enrichment during melt evolution, resulting in a change in the crystallization of quartz by albite as liquidus phases (Manning, 1982). Moreover, the exsolution of the hydrosaline fluid/melt in the terms mentioned above requires a melt enriched in F (Gramenitskiy and Shekina, 1994). Evidence has been found of some enrichment in F in the most apical zone of the Penouta leucogranite, where scarce fluorite and scarce, F-enriched apatite occur (Llorens González *et al*., 2017); the rest of the deposit is heavily depleted in F, and the only mineral phase containing this element is apatite, an accessory mineral, as can be justified by the extremely low whole-rock P_2O_5 contents (~0.02%, Table 1). Besides, the fluorine enrichment in the apical zone could also be justified in terms of the melt evolution itself, as F is an incompatible element (London *et al*., 1988) tending to concentrate in the residual melt.

Furthermore, a scenario of exsolution of a F-enriched hydrosaline fluid/melt triggering an enrichment in Ta in the residual silicate melt could explain the normal zoning of CGM, but it remains unclear whether Ta enrichment, or Nb depletion, which accompany the micro holes in the sponge-like textures are consistent with the exsolution process itself, as the exsolved fluid is enriched in Nb and not in Ta. The latter, linked to the scant evidence of F enrichment in the Penouta deposit, the possibility of a fractional crystallization process as an alternative to explain Nb/Ta, Zr/Hf ratios, and the evolution of Y and *REE* lead us to conclude that the formation of an F-enriched, hydrosaline, low-viscosity melt cannot be justified easily in the Penouta leucogranite on a deposit scale, as for other rare-metal granites that are F, P-rich, e.g. those from the Krásno-Horní Slavkov ore district (René and Škoda, 2011) or in ongoites from the Xianghualing tin district (Huang *et al*. 2002). In the Penouta deposit, the exsolution of a F-bearing melt could only be feasible at a very specific level where the melt, by maximum degree of evolution, would have a significant amount of F (e.g. in the most apical zone where fluorite occurs).

(c) The role played by Cl-bearing fluids

Another possible explanation for the sponge-like textures related to the melt evolution is a Cl-enriched fluid/vapour. The existence of such a fluid is checked easily by an anomalous enrichment in elements that can be mobilized with Cl, as is the case for Sn. This separated Cl-bearing fluid/vapour seems to have occurred in the central part of the Penouta granite body, where there is an enrichment of Sn and Be, and a lack of concomitant enrichment in other elements typically of the evolution of the melt (e.g. Ta, Y and Gd) which would support the notion that degassing processes occurred (see trend II in Fig. 11). Similar conclusions can be drawn for the upper part of the granite body, where some samples of the leucogranite exhibit a dramatic Sn enrichment collinear with the Sn enrichment trend of the central part of the granite (Fig. 11). There is evidence of this separated Cl-bearing fluid in the greisen, where a strong enrichment in Sn occurs with the smallest increase in Ta (trend III, Fig. 11),

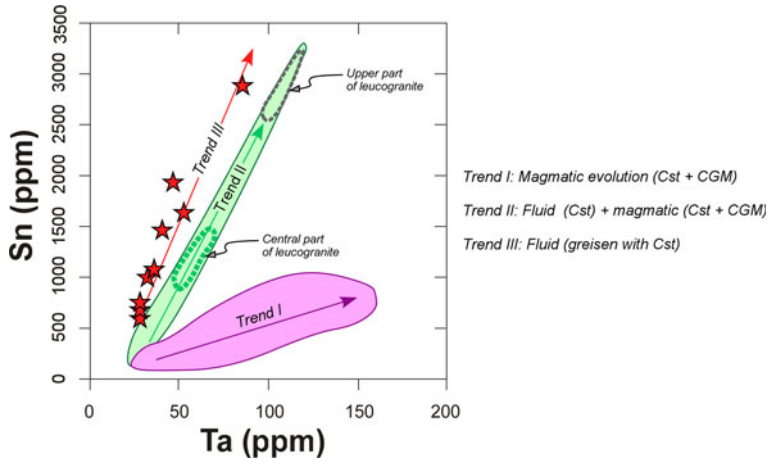

FIG. 11. Trends in variation of the Ta *vs.* Sn contents in the Penouta deposit.

supporting the notion that Ta in the greisen is hosted exclusively by cassiterite, whereas Ta in the leucogranite is hosted by CGM and to a lesser extent by cassiterite (trends I and II in Fig. 10). This fluid/vapour as a metasomatizing agent would probably behave differently in the central part relative to the upper level of the granite. In the central part, the fluid separated from lower levels was probably resorbed in the hot melt when it reached the central part, and only geochemical fingerprints can be found of this process. In contrast, in the upper level the fluid found a solid rock (country rock) and solidified granite, enhancing metasomatic processes on the solidified granite in the most apical zone and the formation of the greisen on the cooler country rock. The different behaviours of the exsolved fluid depending on the area where it is produced could explain that CGM with sponge-like textures are specifically located in the upper part of the granite and are missing in the central part of the Penouta granite.

Experimental constraints seem to support the suggestion that the mobility of Nb might be greater than that of the Ta in an aqueous solution at very low pH (2) and high-temperature conditions (>200°C) (Zaraisky *et al*., 2010; Ballouard *et al*., 2016*b*; Timofeev *et al*., 2017). Therefore, the existence of a Cl-Sn-Be-bearing fluid/vapour separated from the melt could replace previous CGM grains, contribute to the developing of sponge-like textures and the formation of Nb-depleted areas around micro holes as long as this fluid had adequate acidity conditions.

(2) Processes unrelated to the evolution of the melt

It cannot be ruled out that the sponge-like textures could be related to a fluid unrelated to the magmatic evolution, as the Ta-rich rims in CGM could be much younger than the cores (see the geochronological results obtained by Melcher *et al*., 2015), but no tests on the geochronological constraints have been carried out on the Penouta granite to check this possibility. If a long time gap between the formation of the cores and the rims was revealed then the formation of kaolinite might explain this texture, as microthermometry constraints indicate that this process is related to a fluid unrelated to magmatic evolution (Mangas and Arribas, 1991). Besides, the mineral where these textures occur is located at the top of the Penouta granite.

Ta-rich mineral formation

Ta-rich minerals, such as microlite, tapiolite and wodginite, are extremely scarce in the deposit and occur specifically in the apical zone of the leucogranite. Texturally, they seem to be late mineral phases, nucleated on previous CGM crystals and to resemble secondary minerals (see Fig. 6).

A magmatic scenario, in which a melt evolves upwards, fractionating white mica, could lead to a residual liquid rich in Ta (see above), the nucleation of rims of tantalite and ultimately to the formation of other more Ta-enriched minerals. However, the interstitial and secondary aspect of most of these minerals seems to involve an environment with fluids for their formation. It is likely, therefore, that

the formation of Ta-rich minerals is related to a fluid capable of leaching more Nb than Ta from previous CGM crystals, in a similar fashion to that proposed for the formation of the sponge-like textures. The difference between the formation of sponge-like textures and Ta-rich minerals could be a consequence of more fluid–rock interaction in cases where the Ta-rich minerals were formed.

Two points to take into account here are the availability of Nb and Ta and the mobility of the hydrosaline phase. Firstly, enrichment in volatile elements (Li, P, F) in the melt increase the solubility of Na and Ta (Li *et al*., 2015). These volatile elements increase in the late stages of magmatic crystallization, which could lead to the start of the dissolution of early-formed columbite.

With regard to mobility, the phase responsible for the metasomatic transformations must be able to move easily. The hydrosaline phase was defined as a melt rich in fluxing elements such as Cl, Li and F; these are fluxing elements which are poorly soluble in aluminosilicate melt and fractionate to the hydrosaline phase causing its low viscosity (Veksler, 2004; Linnen and Cuney, 2005). In such conditions this magma could move easily and produce metasomatism during its interaction with the early-formed minerals. The metasomatic changes cause albitization and the replacement of Nb-rich oxide minerals by Ta-rich phases such as tantalite, microlite and wodginite. Hydrosaline melts could then be responsible for metasomatic events such as albitization and Ta replacements. The occurrence of fluorite in the apical part of the Penouta deposit suggests a fluorine-rich magma but it was probably released from the magma to the host rocks. Two other elements that play a role in increasing the solubility of H_2O (and thereby in reducing the viscosity) are P and B (Holtz, *et al*., 1993; London, 2015). The Penouta leucogranite is poor in B, and so the formation of a hydrosaline, low-viscosity melt cannot be justified easily as in other rare-metal granites that are F, P-rich, such as those from the Krásno-Horní Slavkov ore district (René and Škoda, 2011) or in ongoites from the Xianghualing tin district (Huang *et al*. 2002).

The overgrowths of tantalite on columbite from the Penouta leucogranite, as well as in other granites (Dostal *et al*., 2015) could be interpreted differently from the Ta-rich rims that formed in a continuous mineral crystallization, however. Melcher *et al*. (2015) dated grains of CGM which had Ta-rich overgrowths and found different ages, 2000 Ma and 2487 Ma, respectively. Similar overgrowths were attributed to the Ta-rich crystallization from a hydrothermal late fluid in granites, e.g. the Nb-Ta-Sn-W-Zr mineralization of the Songshugang granite (Zhu *et al*., 2015), or in pegmatites (Neiva *et al*., 2015). These overgrowths could then have been formed during the magmatic hydrothermal transition (Ballouard *et al*., 2016*a*,*b*).

Moreover, the existence of a fluid/vapour separated from the melt cannot be ruled out in the Penouta granite (López Moro *et al*., 2017). The occurrence of aplite-pegmatites in the upper margin of the granite body, together with the development of the greisen in the country rock, support the separation of a fluid/vapour in the apical part of the granite, where the samples studied were collected. This fluid could contribute to the development of sponge-like textures in some columbite–tantalite crystals and might also favour the leaching of Nb in the crystal rim due to the preferential mobilization of Nb relative to Ta in a fluid (Zaraisky *et al*., 2010; Ballouard *et al*., 2016*b*), resulting in zoned crystals with a Ta-rich rim.

Conclusions

Tantalum in the Sn-Ta Penouta deposit occurs in a highly evolved leucogranite. The main Ta ore in the upper level of the granite is manganocolumbite and manganotantalite with minor amounts of microlite, wodginite and tapiolite, the latter two are mentioned at this location for the first time.

Ta and Ta/Nb variations in the cores of CGM from the Penouta granite are good tools for deciphering the evolution of the melt, revealing an evolution of the melt upwards, which is concomitant with the evolution of the melt inferred by whole-rock geochemistry. However, the whole-rock geochemistry shows that CGM did not fractionate Ta or Nb in the melt, as they probably precipitated in a trapped liquid. As a result, variations of Ta and Nb in cores of CGM depended on the fractionation of essential minerals, especially muscovite, which is able to fractionate Nb relative to Ta. This observation, together with the existence of normal and oscillatory zoning in CGM, indicates that these phases crystallized from a melt.

Similarly to other rare-metal leucogranites, a subsequent important fluid activity occurred in the Penouta albite leucogranite, resulting in the development of sponge-like textures and depletions of Nb in the CGM. Experimental constraints seem to suggest that a fluid under certain conditions of acidity and temperature could cause partial digestion of the CGM and greater solubility of Nb than Ta. There is evidence of Cl-Sn-Be-bearing fluids exsolved from the melt, probably with very-low pH

conditions, affecting the central and the upper levels of the leucogranite and the country rock (greisen) that is most likely to explain the formation of sponge-like textures and the leaching of Nb in CGM. Similarly, the formation of interstitial Ta-enriched minerals (microlite, tapiolite and wodginite) could respond to the same phenomenon as sponge-like textures, but with a greater degree of fluid–rock interaction.

Acknowledgements

This work is part of the project H2020-642201-OptimOre financed by the European Union. Ana Domingo and Eva Prats assisted with the SEM study and Xavier Llovet with the microprobe analyses. The authors thank 'Strategic Minerals Spain' for supporting the sampling. They are also grateful to the Guest Prinicpal Editor J. Bowles, Guest Associate Editor E. Deady, and to R.A. Shaw and two other anonymous reviewers for their valuable comments.

References

Abdalla, H.M., Helba, H.A. and Mohamed, F.H. (1998) Chemistry of columbite-tantalite minerals in rare metal granitoids, Eastern Desert, Egypt. *Mineralogical Magazine*, **62**, 821–836.

ACTLABS (2017) Activation Laboratories Schedule of services. [Available from http://www.actlabs.com/files/Actlabs_-_Schedule_of_Services_-_Euro_-_2017-09-15.pdf] (Accessed November 2017).

Alfonso, P. and Melgarejo, J.C. (2008) Fluid evolution in the zoned rare-element pegmatite field at Cap de Creus, Catalonia, Spain. *The Canadian Mineralogist*, **46**, 597–617.

Alfonso, P., Corbella, M. and Melgarejo, J.C. (1995) Nb-Ta-minerals from the Cap de Creus pegmatite field, eastern Pyrenees: distribution and geochemical trends. *Mineralogy and Petrology*, **55**, 53–69.

Anderson, M.O., Lentz, D.R., McFarlane, M. and Falck, H. (2013) A geological, geochemical and textural study of a LCT pegmatite: implications for the magmatic versus metasomatic origin of Nb–Ta mineralization in the Moose II pegmatite, Northwest Territories. *Journal of Geosciences*, **58**, 299–320.

Arias, D., Farias, P. and Marcos, A. (2002) Estratigrafía y estructura del Antiforme del Ollo de Sapo en el área de Viana do Bolo-A Gudiña (Provincia de Orense, NO de España): nuevos datos sobre la posición estratigráfica de la Formación porfiroide Ollo de Sapo. *Trabajos de Geología*, **23**, 9–19.

Arribas, A. and Mangas, J. (1991) Fluid inclusion study of tin-mineralized greisens and quartz veins in the Penouta apogranite (Orense, Spain). *Mineralogical Magazine*, **55**, 211–223.

Assadzadeh, G.E., Samson, I.M. and Gagnon, J.E. (2017) Evidence for aqueous liquid-liquid immiscibility in highly evolved tin-bearing granites, Mount Pleasant, New Brunswick, Canada. *Chemical Geology*, **448**, 123–136.

Badanina, E.V., Veksler, I.V., Thomas, R., Syritso, L.F. and Trumbull, R.B. (2004) Magmatic evolution of Li–F, rare-metal granites: a case study of melt inclusions in the Khangilay complex, Eastern Transbaikalia (Russia) *Chemical Geology*, **210**, 113–133.

Bacon, C.R. (1989) Crystallization of accessory phases in magmas by local saturation adjacent to phenocrysts. *Geochimica et Cosmochimica Acta*, **53**, 1055–1066.

Ballouard, C., Marc Poujol, M., Boulvais, P., Branquet, Y., Tartèse, R. and Vigneresse, J. (2016*a*) Nb–Ta fractionation in peraluminous granites: a marker of the magmatic–hydrothermal transition. *Geology*, **44**, 231–234.

Ballouard, C., Marc Poujol, M., Boulvais, P., Branquet, Y., Tartèse, R. and Vigneresse, J. (2016*b*) Nb-Ta fractionation in peraluminous granites: A marker of the magmatic-hydrothermal transition: REPLY. *Geology*, **44**, e395.

Belkasmi, M. and Cuney, M. (1998) Les columbo-tantalites zones du granite de Montebras (Massif central, Français) Implications pétrogénétiques. *Comptes Rendus de l'Académie des Sciences-Series IIA-Earth and Planetary Science*, **326**, 459–465.

Belkasmi, M., Cuney, M., Pollard, P.J. and Bastoul, A. (2000) Chemistry of the Ta-Nb-Sn-W oxide minerals from the Yichun rare metal granite (SE China): genetic implications and comparison with Moroccan and French Hercynian examples. *Mineralogical Magazine*, **64**, 507–523.

Bleischwitz, R., Dittrich, M. and Pierdicca, C. (2012) Coltan from Central Africa, international trade and implications for any certification. *Resources Policy*, **37**, 19–29.

Canosa, F., Martín-Izard, A. and Fuertes-Fuente, M. (2012) Evolved granitic system as a source of rare-element deposits: The Ponte Segade case (Galicia, NW Spain). *Lithos*, **153**, 165–176.

Černý, P. (1989) Exploration strategy and methods for pegmatite deposits of tantalum. Pp. 274–302 in: *Lanthanides, Tantalum and Niobium* (P. Moller, P. Černý and F. Saupe, editors). Springer-Verlag, New York.

Černý, P. and Ercit, T.S. (1989) Mineralogy of niobium and tantalum: crystal chemical relationships, paragenetic aspects and their economic implications. Pp. 27–79 in: *Lanthanides, Tantalum and Niobium* (P. Moller, P. Černý and F. Saupe, editors). Springer-Verlag, New York.

Černý, P., Roberts, W.L., Ercit, T.S. and Chapman, R. (1985) Zirconium and hafnium in minerals of the columbite and wodginite groups from granitic pegmatites. *The Canadian Mineralogist*, **45**, 185–202.

Černý, P., Chapman, R., Ferreira, K., Smeds and S.A. (2004) Geochemistry of oxide minerals of Nb, Ta, Sn, and Sb in the Varuträsk granitic pegmatite, Sweden: The case of an "anomalous" columbite-tantalite trend. *American Mineralogist*, **89**, 505–518.

Černý, P., Blevin, P.L., Cuney, M. and London, D. (2005) *Granite-related ore deposits*. Economic Geology 100th Anniversary Volume, 337–370.

Černý, P., Ercit, T.S., Smeds, S.A., Groat, L.A. and Chapman, R. (2007) Wodginite and associated oxide rninerals from the Peerless pegmatite, Pennington County, South Dakota. *American Mineralogist*, **70**, 1044–1049.

Charoy, B. and Noronha, F. (1996) Multistage growth of a rare-element, volatile-rich microgranite at argemela (Portugal). *Journal of Petrology*, **37**, 73–94.

Chicharro, E., Martín-Crespo, T., Gómez-Ortiz, D., López-García, J.A., Oyarzun, R. and Villaseca, C. (2015) Geology and gravity modeling of the Logrosán Sn–(W) ore deposits (Central Iberian Zone, Spain). *Ore Geology Reviews*, **65**, 294–307.

Clauer, N., Fallick, A.E., Galán, E., Aparicio, P., Miras, A., Fernández-Caliani, J.C. and Aubert, A. (2015) Stable isotope constraints on the origin of kaolin deposits from Variscan granitoids of Galicia (NW Spain). *Chemical Geology*, **417**, 90–101.

Cuney, M., Marignac, C. and Weisbrod, A. (1992) The Beauvoir topaz–lepidolite albite granite (Massif Central, France); the disseminated magmatic Sn–Li–Ta–Nb–Be mineralization. *Economic Geology*, **87**, 1766–1794.

Dewaele, S., Hulsbosch, N., Cryns, Y., Boyce, A., Burgess, R. and Muchez, Ph. (2015) Geological setting and timing of the world-class Sn, Nb–Ta and Li mineralization of Manono-Kitotolo (Katanga, Democratic Republic of Congo). *Ore Geology Reviews*, **72**, 373–390.

Díez, A., Martínez Catalán, J.R. and Bellido Mulas, F. (2010) Role of the Ollo de Sapo massive felsic volcanism of NW Iberia in the Early Ordovician dynamics of northern Gondwana. *Gondwana Research*, **17**, 363–376.

Díez Montes, A. (2006) *La Geología del Dominio "Ollo de Sapo" en las comarcas de Sanabria y Terra do Bolo*. (Geology of the "Ollo de Sapo" domain in the Sanabria and Terra do Bolo regions). *PhD thesis*, University of Salamanca-IGME, Spain.

Dill, H.G., Dohrmann, R., Kaufhold, S. and Balaban, S.I. (2015) Kaolinization – a tool to unravel the formation and unroofing of the Pleystein pegmatite–aplite system (SE Germany). *Ore Geology Reviews*, **69**, 33–56.

Dostal, J., Kontak, D.J., Gerel, O., Shellnutt, J.G. and Fayek, M. (2015) Cretaceous ongonites (topaz-bearing albite-rich microleucogranites) from Ongon Khairkhan, Central Mongolia: Products of extreme magmatic fractionation and pervasive metasomatic fluid:rock interaction. *Lithos*, **236–237**, 173–189.

Ercit, T.S., Hawthorne, F.C. and Černý, P. (1992*a*) The wodginite group. I. Structural crystallography. The *Canadian Mineralogist*, **30**, 597–611.

Ercit, T.S., Černý, P., Hawthorne, F.C. and McGammon, C.A. (1992*b*) The wodginite group. II. Crystal chemistry. The *Canadian Mineralogist*, **30**, 613–631.

Ercit, T.S., Černý, P. and Hawthorne, F.C. (1992*c*) The wodginite group. III. Classification and new species. The *Canadian Mineralogist*, **30**, 633–638.

Ferragne, A. (1972) *Le Précambrien et le paleozoïque de la province d'Orense (nord-ouest de l'Espagne)*. Stratigraphie-tectonique-métamorphisme. *PhD thesis*, University of Bordeaux, France, 249 pp.

Galliski, M.A., Márquez-Zavalia, M.F., Černý, P., Martínez, V.A. and Capman, R. (2008) The Ta-Nb-Sn-Ti oxide-mineral paragenesis from La Viquita, a spodumene-bearing rare-element granitic pegmatite, San Luis, Argentina. The *Canadian Mineralogist*, **30**, 379–393.

Gonzalo Corral, F.J. and Gracía Plaza, A.S. (1985) Yacimientos de estaño del oeste de España: Ensayo de caracterización y clasificación económicas. *Cuadernos do Laboratorio Xeologico de Laxe*, **9**, 265–303.

Gramenitskiy, Y.N. and Shekina, T.I. (1994) Phase relationships in the liquidus part of a granitic system containing fluorine. *Geochemistry International*, **31**, 52–70.

Gutiérrez-Alonso, G., Collins, A.S., Fernández-Suárez, J., Pastor-Galán, D., González-Clavijo, E., Jourdan, F., Weil, A.B. and Johnston, S.T. (2015) Dating of lithospheric buckling: $^{40}Ar/^{39}Ar$ ages of syn-orocline strike–slip shear zones in northwestern Iberia. *Tectonophysics*, **643**, 44–54.

Helba, H., Trumbull, R.B., Morteani, G., Khalil, S.O. and Arslan, A. (1997) Geochemical and petrographic studies of Ta mineralization in the Nuweibi albite granite complex, Eastern Desert, Egypt. *Mineralium Deposita*, **32**, 164–179.

Holtz, F., Dingwell, D.B. and Behrens, H. (1993) Effects of F, B_2O_3, and P_2O_5 on the solubility of water in haplogranite melts compared to natural silicate melts. *Contributions to Mineralogy and Petrology*, **113**, 492–501.

Huang, X.L., Wang, R.C., Chen, X.M., Hu, H. and Liu, C. S. (2002) Vertical variations in the mineralogy of the Yichun topaz–lepidolite granite, Jiangxi Province, southern China. *The Canadian Mineralogist*, **40**, 1047–1068.

Huang, F.F., Wang, R.C., Xie, L., Zhu, J.C., Erdmann, S., Che, X.D. and Zhang, R.Q. (2015) Differentiated rare-element mineralization in an ongonite–topazite composite dike at the Xianghualing tin district, Southern China: An electron-microprobe study on the evolution from niobium–tantalum-oxides to cassiterite. *Ore Geology Reviews*, **65**, 761–778.

IGME (1976) Estudio básico de los yacimientos de estaño tipo-Penouta. Internal review. Pp. 166.

Iglesias, M. and Choukroune, P. (1980) Shear zones in the Iberian Arc. *Journal of Structural Geology*, **114**, 63–68.

Julivert, M., Fontboté, J.M., Ribeiro, A. and Nabais Conde, L.E. (1972) *Mapa Tectónico de la Península Ibérica y Baleares E.1:1.000.000*. IGME, Madrid.

Kamenetsky, V.S., Naumovc, V.B., Davidsona, P., van Achterberghd, E. and Ryan, C.G. (2004) Immiscibility between silicate magmas and aqueous fluids: a melt inclusion pursuit into the magmatic-hydrothermal transition in the Omsukchan Granite (NE Russia). *Chemical Geology*, **210**, 73–90.

Keppler, H. (1993) Influence of fluorine on the enrichment of high field strength trace elements in granitic rocks. *Contributions to Mineralogy and Petrology*, **114**, 479–488.

Lahti, S.I. (1987) Zoning in columbite–tantalite crystals from the granitic pegmatites of the Erajarvi area, southern Finland. *Geochimica et Cosmochimica Acta*, **51**, 509–517.

Li, J., Huang, X.L., He, P.L., Li, W.X., Li, W.X., Yu, Y. and Cheng, L.L. (2015) In situ analyses of micas in the Yashan granite, South China: Constraints on magmatic and hydrothermal evolutions of W and Ta–Nb bearing granites. *Ore Geology Reviews*, **65**, 793–810.

Linnen, R.L. (1998) The solubility of Nb–Ta–Zr–Hf–W in granitic melts with Li and Li + F: constraints for mineralization in rare metal granites and pegmatites. *Economic Geology*, **93**, 1013–1025.

Linnen, R.L. and Cuney, M. (2005) Granite-related rare-element deposits and experimental constraints on Ta-Nb-W-Sn-Zr-Hf mineralization. Pp. 45–68. In: *Rare Element Geochemistry and Mineral Deposits* (R.L. Linnen and I.M. Samson, editors). Geological Association of Canada Short Course Notes, **17**.

Linnen, R.L. and Keppler, H. (1997) Columbite solubility in granitic melts: consequences for the enrichment and fractionation of Nb and Ta in the Earth's crust. *Contributions to Mineralogy and Petrology*, **128**, 213–227.

Linnen, R.L., Samson, I.M., Williams-Jones, A.E. and Chakhmouradian, A.R. (2014) Geochemistry of the Rare-Earth Element, Nb, Ta, Hf, and Zr Deposits. Pp. 543–564 in: *Treatise on Geochemistry* (H.D. Holland and K.K. Turekian, editors). 2nd edition **Vol. 13**, Elsevier, Oxford.

London, D. (2008) *Pegmatites*. The Canadian Mineralogist, Spec. Publ., **10**, 347 pp.

London, D. (2015) Reply to Thomas and Davidson on "A petrologic assessment of internal zonation in granitic pegmatites" (London, 2014a). *Lithos*, **212–215**, 469–484.

London, D., Hervig, R.L. and Morgan, G.B. (1988) Melt-vapor solubilities and elemental partitioning in peraluminous granite-pegmatite systems: experimental results with Macusani glass at 200 MPa. *Contributions to Mineralogy and Petrology*, **99**, 360–373.

Llorens, T. and Moro, M.C. (2010) Microlite and tantalite in the LCT granitic pegmatites of La Canalita, Navasfrías Sn-W District, Salamanca, Spain. The *Canadian Mineralogist*, **48**, 549–564.

Llorens, T. and Moro, M.C. (2012) Oxide minerals in the granitic cupola of the Jálama Batholith, Salamanca, Spain. Part I: accessory Sn, Nb, Ta and Ti minerals in leucogranites, aplites and pegmatites. *Journal of Geosciences*, **57**, 25–43.

Llorens González, T., García Polonio, F., López Moro, F. J., Fernández-Fernández, A., Sans Contreras, J.L. and Moro Benito, M.C. (2017) Tin-tantalum-niobium mineralization in the Penouta deposit (NW Spain): Textural features and mineral chemistry to unravel the genesis and evolution of cassiterite and columbite group minerals in a peraluminous system. *Ore Geology Reviews*, **81**, 79–95.

López Moro, F.J., García Polonio, F., Llorens González, T., Sanz Contreras, J.L., Fernández-Fernández, A. and Moro Benito, M.C. (2017) Ta and Sn concentration by muscovite fractionation and degassing in a lens-like granite body: The case study of the Penouta rare-metal albite granite (NW Spain). *Ore Geology Reviews*, **82**, 10–30.

Mackay, A.R. and Simandl, G.J. (2014) Geology, market and supply chain of niobium and tantalum – a review. *Mineralium Deposita*, **49**, 1025–1047.

Mangas, J. and Arribas, A. (1991) Fluid inclusion study of tin-mineralized greisens and quartz veins in the Penouta apogranite (Orense, Spain). *Mineralogical Magazine*, **55**, 211–223.

Manning, D.A.C. (1982) An experimental study of the effects of fluorine on the crystallization of granitic melts. Pp. 191–203 in: *Metallization Associated with Acid Magmatism* (A.M. Evans, editor). John Wiley & Sons, New York.

Martins, T., Lima, A., Simmons, W.B., Falster, U. and Noronha, F. (2011) Geochemical fractionation of Nb–Ta oxides in Li-bearing pegmatites from the Barroso–Alvão pegmatite field, Northern Portugal. The *Canadian Mineralogist*, **49**, 777–791.

Masau, M., Černý, P. and Chapman, R. (2000) Exsolution of zirconian-hafnian wodginite from manganoan-tantalian cassiterite, Annie claim #3 granitic pegmatite, Southeastern Manitoba, Canada. The *Canadian Mineralogist*, **38**, 685–694.

Melcher, F., Graupner, T., Gäbler, H.E., Sitnikova, M., Henjes-Kunst, F., Oberthür, T., Gerdes, A. and Dewaele, S. (2015) Tantalum-(niobium–tin) mineralisation in African pegmatites and rare metal granites: constraints from Ta–Nb oxide mineralogy, geochemistry and U–Pb geochronology. *Ore Geology Reviews*, **64**, 667–719.

Neiva, A.M.R., Gomes, M.E.P., Ramos, J.M.F. and Silva, P.B. (2008) Geochemistry of granitic aplite-pegmatite sills and their minerals from Arcozelo da Serra area

(Gouveia, central Portugal). *European Journal of Mineralogy*, **20**, 465–485.

Neiva, A.M.R., Gomes, M.E.P. and Silva, P.B. (2015) Two generations of zoned crystals of columbite-group minerals from granitic aplite–pegmatite in the Gouveia area, central Portugal. *European Journal of Mineralogy*, **27**, 771–482.

Pollard, P.J., Pichavant, M. and Charoy, B. (1987) Contrasting evolution of fluorine and boron-rich tin systems. *Mineralium Deposita*, **22**, 315–321.

Raimbault, L. and Burnol, L. (1998) The Richemont rhyolite dyke (French Massif Central): a subvolcanic equivalent of rare-metal granites. *The Canadian Mineralogist*, **36**, 265–282.

Rao, C., Wang, R.C., Hu, H. and Zhang, W.L. (2009) Complex internal textures in oxide minerals from the Nanping no. 31 dyke of granitic pegmatite, Fujian province, Southeastern China. *The Canadian Mineralogist*, **47**, 1195–1212.

René, M. and Škoda, R. (2011) Nb-Ta-Ti oxides fractionation in rare-metal granites: Krásno-Horní Slavkov ore district, Czech Republic. *Mineralogy and Petrology*, **103**, 37–48.

Roedder, E. (1992) Fluid inclusion evidence for immiscibility in magmatic differentiation. *Geochimica et Cosmochimica Acta*, **56**, 5–20.

Roskill Information Services Ltd. (2016) *Tantalum: Global Industry, Markets and Outlook to 2020*. Roskill, London, 12th edition.

Rub, A.K., Štemprok, M. and Rub, M.G. (1998) Tantalum mineralization in the apical part of the Cinovec (Zinnwald) granite stock. *Mineralogy and Petrology*, **63**, 199–202.

Selway, J., Breaks, F.W. and Tindle, A.G. (2005) A review of rare-element (Li-Cs-Ta) pegmatite exploration techniques for the Superior Province, Canada, and large worldwide tantalum deposits. *Exploration and Mining Geology*, **14**, 1–30.

Shore, M. and Fowler, A.D. (1996) Oscillatory zoning in minerals; a common phenomenon. *The Canadian Mineralogist*, **34**, 1111–1126.

Smith, E.K., Cazier, J.A., Fox, J. and Kitunda, J.M. (2012) The effect of child labour in Africa on consumers of the cell phone industry. *International Journal of Information Systems and Change Management*, **6**, 147–159.

Spilde, N. and Shearer, C.K. (1992) A comparison of tantalum-niobium oxide assemblages in two mineralogically distinct rare-element granitic pegmatites, Black Hills, South Dakota. *The Canadian Mineralogist*, **30**, 719–737.

Stepanov, A., Mavrogenes, J.A., Meffre, S. and Davidson, P. (2014) The key role of mica during igneous concentration of tantalum. *Contributions to Mineralogy and Petrology*, **167**, 1–8.

Tadesse, S. and Zerihun, D. (1996) Composition, fractionation trend and zoning accretion of the columbite-tantalite group of minerals in the Kenticha rare-metal field (Adola, southern Ethiopia). *Journal of African Earth Sciences*, **23**, 411–431.

Tartèse, R. and Boulvais, P. (2010) Differentiation of peraluminous leucogranites "en route" to the Surface. *Lithos*, **114**, 353–368.

Thomas, R. and Davidson, P. (2013) The missing link between granites and granitic pegmatites. *Journal of Geosciences*, **58**, 183–200.

Timofeev, A., Migdisov, A.A. and Williams-Jones, A.E. (2017) An experimental study of the solubility and speciation of tantalum in fluoride-bearing aqueous solutions at elevated temperature. *Geochimica et Cosmochimica Acta*, **197**, 294–304.

Tindle, A.G. and Breaks, F.W. (2000) Columbite-tantalite mineral chemistry from rare element granitic pegmatites: Separation Lake area, NW Ontario, Canada. *Mineralogy and Petrology*, **70**, 165–198.

Uher, P., Žitňan, P. and Ozdín, D. (2007) Pegmatitic Nb-Ta oxide minerals in alluvial placers from Limbach, Bratislava Massif, Western Carpathians, Slovakia: Compositional variations and evolutionary trend. *Journal of Geosciences*, **52**, 133–141.

Vegas, N., Aranguren, A., Cuevas, J. and Tubía, J.M. (2001) Variaciones en los mecanismos de emplazamiento de los granitos del eje Sanabria-Viana do Bolo (Macizo Ibérico, España). *Boletín Geológico y Minero*, **112**, 79–88.

Veksler, I.V. (2004) Liquid immiscibility and its role at the magmatic–hydrothermal transition: a summary of experimental studies. *Chemical Geology*, **2010**, 7–31.

Webster, J.D., Vetere, F., Botcharnikov, R.E., Goldoff, B., McBirney, A. and Doherty, A.L. (2015) Experimental and modeled chlorine solubilities in aluminosilicate melts at 1 to 7000 bars and 700 to 1250°C: Applications to magmas of Augustine Volcano, Alaska. *American Mineralogist*, **100**, 522–535.

Wise, M.A. and Brown, C.D. (2010) Mineral chemistry, petrology and geochemistry of the Sebago granite–pegmatite system, southern Maine, USA. *Journal of Geosciences*, **55**, 3–26.

Wise, M.A., Černý, P. and Falster, A.U. (1998) Scandium substitution in columbite-group minerals and ixiolite. The *Canadian Mineralogist*, **36**, 673–680.

Zaraisky, G.P., Korzhinskaya, V. and Kotova, N. (2010) Experimental studies of Ta_2O_5 and columbite–tantalite solubility in fluoride solutions from 300 to 550°C and 50 to 100 MPa. *Mineralogy and Petrology*, **99**, 287–300.

Zhu, Z.Y., Wang, R.C., Che, X.D., Zhu, J.C., Wei, X.L. and Huang, X. (2015) Magmatic–hydrothermal rare-element mineralization in the Songshugang granite (northeastern Jiangxi, China): Insights from an electron-microprobe study of Nb–Ta–Zr minerals. *Ore Geology Reviews*, **65**, 749–760.